Article

Immunity

Intestinal Tuft-2 cells exert antimicrobial immunity via sensing bacterial metabolite N-undecanoylglycine

Graphical abstract

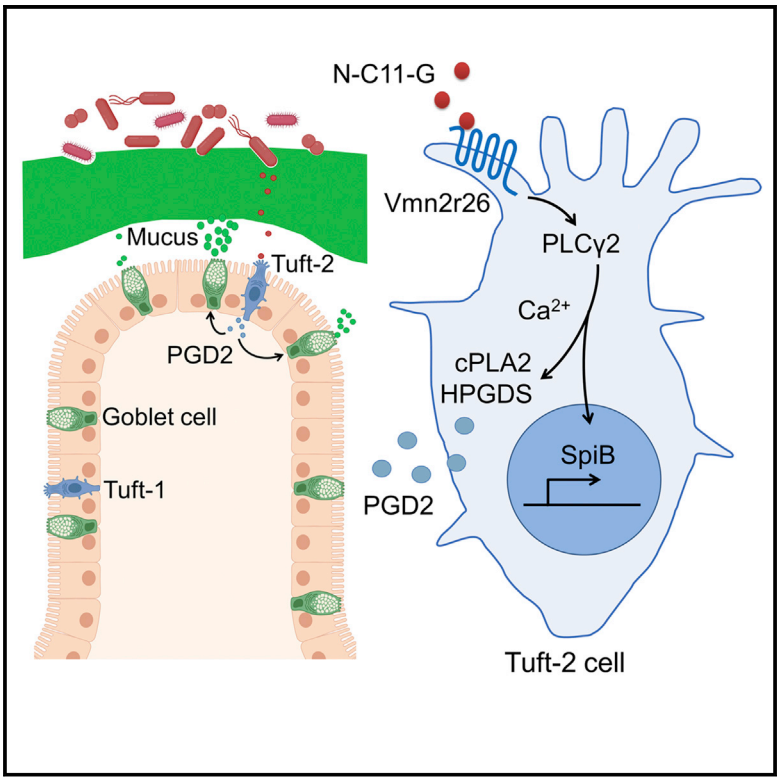

Authors

Zhen Xiong, Xiaoxiao Zhu, Jingjing Geng, ..., Ying Du, Yong Tian, Zusen Fan

Correspondence

ytian@ibp.ac.cn (Y.T.), fanz@moon.ibp.ac.cn (Z.F.)

In brief

Tuft cells play a critical role in immunity against parasite infection, but whether Tuft cells participate in bacterial eradication is presently unclear. Xiong et al. reveal that Tuft-2 cells mediate immunity against bacterial infection through Vmn2r26-mediated recognition of bacterial metabolites.

Highlights

- Tuft-2 cells exert antibacterial function
- Tuft-2 cells sense bacterial metabolites through Vmn2r26
- PGD2 produced by Tuft-2 cells facilitates mucus secretion of goblet cells
- SpiB is required for Tuft-2 cell expansion over bacterial infection

Xiong et al., 2022, Immunity *55*, 686–700
April 12, 2022 © 2022 Elsevier Inc.
https://doi.org/10.1016/j.immuni.2022.03.001

CellPress

CellPress

Immunity

Article

Intestinal Tuft-2 cells exert antimicrobial immunity via sensing bacterial metabolite N-undecanoylglycine

Zhen Xiong,[1,2,5] Xiaoxiao Zhu,[2,5] Jingjing Geng,[1,4,5] Yuwei Xu,[1,2,3,5] Runyuan Wu,[1,3] Cunzhen Li,[1,3] Dongdong Fan,[2] Xiwen Qin,[1,3] Ying Du,[1] Yong Tian,[2,3,*] and Zusen Fan[1,3,6,*]

[1]Key Laboratory of Infection and Immunity of CAS, CAS Center for Excellence in Biomacromolecules, Institute of Biophysics, Chinese Academy of Sciences, Beijing 100101, China

[2]Key Laboratory of RNA Biology of CAS, Institute of Biophysics, Chinese Academy of Sciences, Beijing, China

[3]University of Chinese Academy of Sciences, Beijing 100049, China

[4]College of Life Sciences, University of Chinese Academy of Sciences, Beijing 100049, China

[5]These authors contributed equally

[6]Lead contact

*Correspondence: ytian@ibp.ac.cn (Y.T.), fanz@moon.ibp.ac.cn (Z.F.)

https://doi.org/10.1016/j.immuni.2022.03.001

SUMMARY

Tuft cells are a type of intestinal epithelial cells that exist in epithelial barriers and play a critical role in immunity against parasite infection. It remains insufficiently clear whether Tuft cells participate in bacterial eradication. Here, we identified Sh2d6 as a signature marker for CD45$^+$ Tuft-2 cells. Depletion of Tuft-2 cells resulted in susceptibility to bacterial infection. Tuft-2 cells quickly expanded in response to bacterial infection and sensed the bacterial metabolite N-undecanoylglycine through vomeronasal receptor Vmn2r26. Mechanistically, Vmn2r26 engaged with N-undecanoylglycine activated G-protein-coupled receptor-phospholipase C gamma2 (GPCR-PLCγ2)-Ca^{2+} signaling axis, which initiated prostaglandin D2 (PGD2) production. PGD2 enhanced the mucus secretion of goblet cells and induced antibacterial immunity. Moreover, Vmn2r26 signaling also promoted SpiB transcription factor expression, which is responsible for Tuft-2 cell development and expansion in response to bacterial challenge. Our findings reveal an additional function of Tuft-2 cells in immunity against bacterial infection through Vmn2r26-mediated recognition of bacterial metabolites.

INTRODUCTION

The mammalian gut is not only an organ of nutrient absorption but also one of the largest peripheral immune organs. Intestinal epithelial cells (IECs) constitute barrier surfaces that separate mammalian hosts from the external environment. IECs sense contents of intestinal lumen, including nutrients, microbiota, and metabolites, crosstalking with immune cells in the lamina propria to orchestrate intestinal homeostasis and immunity. Tuft cells are one type of the epithelial cell and exist in epithelial barriers throughout the body, including the gastrointestinal tract, gall bladder, nasal cavity, trachea, and even thymus (Haber et al., 2017; Miller et al., 2018; Montoro et al., 2018; Schneider et al., 2019). Tuft cells are major source of interleukin-25 (IL-25) in the intestine (Desai et al., 2021; von Moltke et al., 2016). Upon helminth infection, IL-25 produced by Tuft cells further activates group 2 innate lymphoid cells (ILC2) to secrete IL-13, which initiates immune response against parasites. The Tuft cell-ILC2 circuit potentiates intestinal remodeling and mediates type 2 immunity to expulse parasites (Gerbe et al., 2016; Howitt et al., 2016; Schneider et al., 2018). A recent report shows that Tuft cells can synthesize cysteinyl leukotrienes to prime immunity against helminth infection (McGinty et al., 2020).

Intestinal Tuft cells express the succinate receptor (SUCNR1) to sense succinate derived from tritrichomonad and microbiota (Lei et al., 2018; Nadjsombati et al., 2018; Schneider et al., 2018). Tuft cells also express some other G-protein-coupled receptors (GPCRs) such as free fatty acid receptor 3 (FFAR3) and bitter taste receptors (type 2 taste receptors, T2Rs). T2Rs transduce signaling via G protein cascade to activate Tuft cells against *Trichinella spiralis* infection (Luo et al., 2019). Olfactory receptors are another canonical type of chemosensory GPCRs. Vomeronasal receptors (VRs) are a unique class of olfactory receptors for pheromones. VRs are classified into three subfamilies, type I VRs (V1Rs), type II VRs (V2Rs), and formyl peptide receptors (FPRs) (Dalton and Lomvardas, 2015; Rivière et al., 2009). In addition to vomeronasal neuroepithelium, FPRs are expressed in neutrophils and macrophages that recognize bacterial formylated peptides to initiate antimicrobial immunity (Bufe et al., 2019; Weiß and Kretschmer, 2018). However, the function of olfactory receptors in Tuft cells remains elusive.

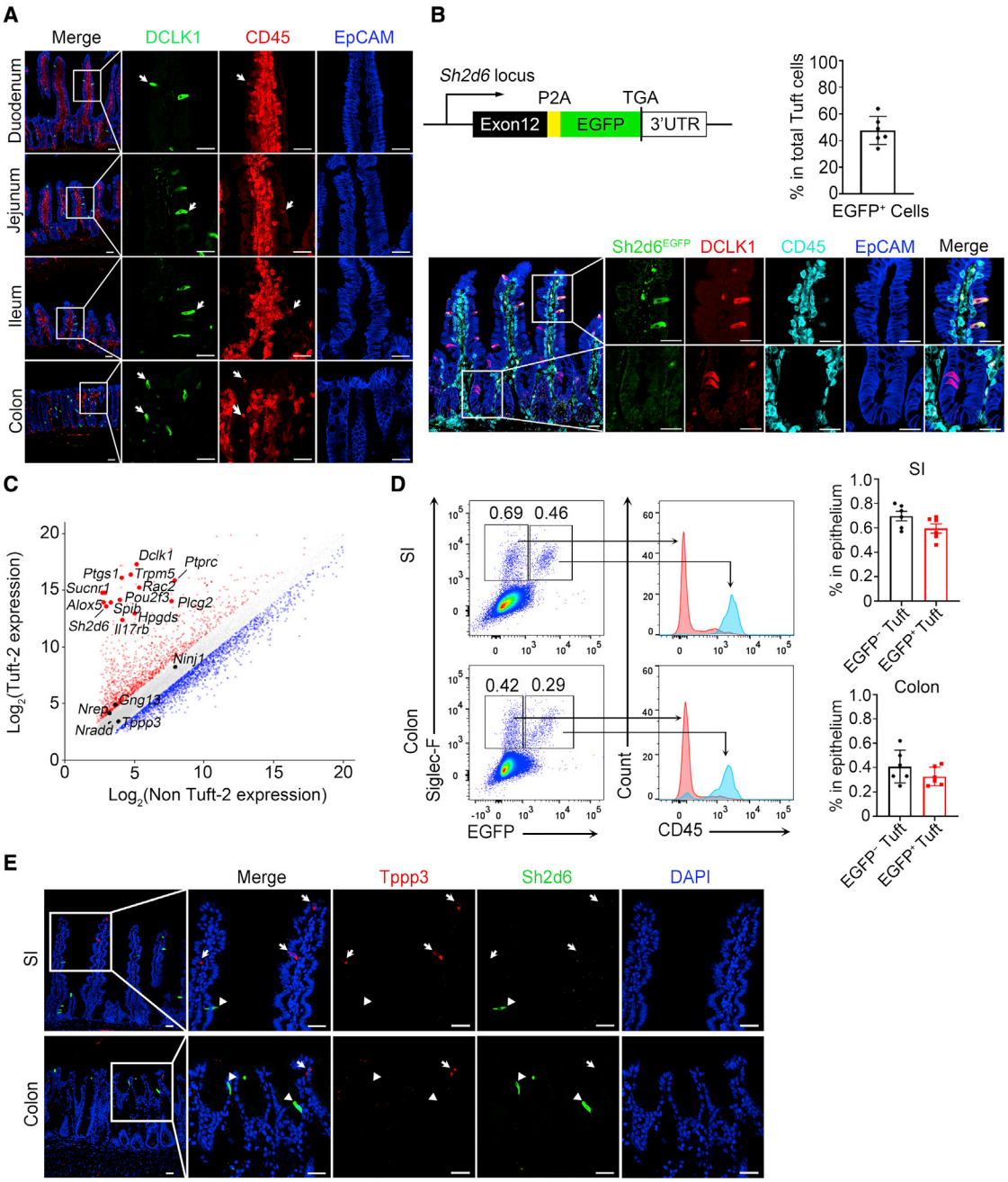

Figure 1. CD45$^+$ Tuft-2 cells exist in intestines

(A) Immunofluorescence staining of CD45$^+$ Tuft-2 cells in duodenum, jejunum, ileum, and colon with DCLK1 (green), CD45 (red), and EpCAM (blue) antibodies. White arrowheads denote CD45$^+$ Tuft-2 cells. Scale bar, 30 μm. Data are representative of three independent experiments.

(B) *Sh2d6*^{EGFP} mice were generated by CRISPR-Cas9 technology. Small intestines of *Sh2d6*^{EGFP} mice were stained with EGFP (green), DCLK1 (red), CD45 (cyan), and EpCAM (blue) antibodies. Representative fields are enlarged. Scale bar, 20 μm. Percentage of EGFP$^+$ cells in total DCLK1$^+$ cells were calculated; n = 6 biological replicates.

(C) Sh2d6$^+$ Tuft-2 cells (EGFP$^+$EpCAM$^+$Siglec-F$^+$) and non-Tuft-2 epithelial cells (EGFP$^-$EpCAM$^+$) were sorted from *Sh2d6*^{EGFP} mice with flow cytometry. RNA was extracted, and transcriptome was analyzed by gene expression microarray. Representative genes are shown.

(D) Flow cytometry analysis of Sh2d6$^+$ Tuft-2 cells (EGFP$^+$EpCAM$^+$Siglec-F$^+$CD45$^+$) and Sh2d6$^-$ Tuft cells (EGFP$^-$EpCAM$^+$Siglec-F$^+$CD45$^-$) in small intestine and colon of *Sh2d6*^{EGFP} reporter mice. Data were pregated from FSC/SSC, singlet, and EpCAM positive classes; n = 6 biological replicates.

(E) Small intestine and colon of Sh2d6-HA mice were stained with HA (for Sh2d6) (green) and Tppp3 (red) antibodies. Nuclei were counterstained with DAPI (blue). White arrowheads indicate Sh2d6$^-$Tppp3$^+$ Tuft-1 cells. Triangles indicate Sh2d6$^+$Tppp3$^-$ Tuft-2 cells. Scale bar, 30 μm. Data are representative of three independent experiments.

Please also see Figures S1 and S2.

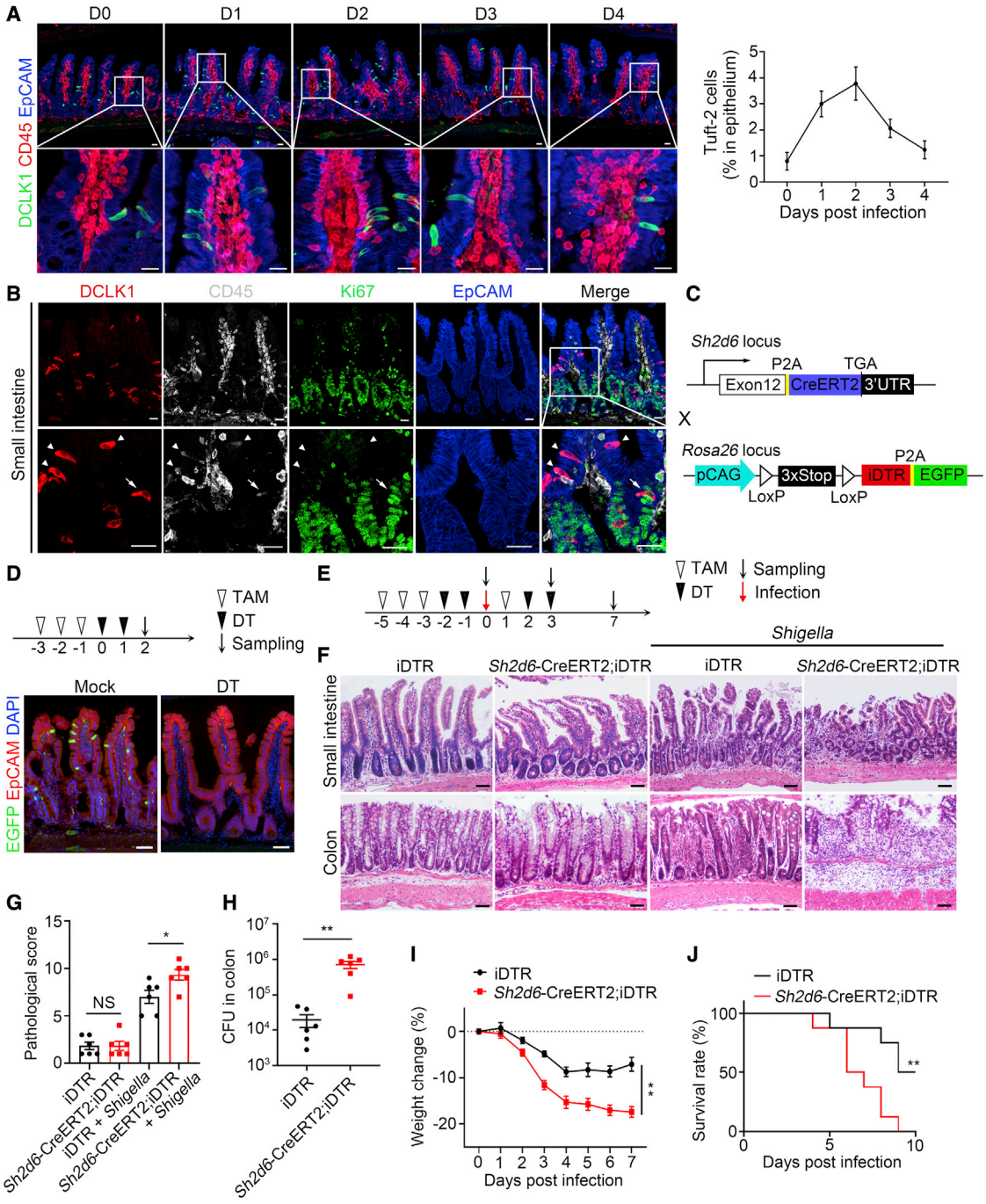

Figure 2. Tuft-2 cell depleted mice are susceptible to *Shigella* infection

(A) Mice were infected with *Shigella* by oral gavage of 5 × 10^7 CFU. Small intestine was collected in indicated days and stained with DCLK1 (green), CD45 (red), and EpCAM (blue) antibodies (left). Scale bar, 20 μm. Percentages of Tuft-2 ($CD45^+DCLK1^+EpCAM^+$) cells in total epithelial cells were calculated (right). 50 crypt-villus units per mouse; n = 4 biological replicates. Data are representative of three independent experiments.

(B) Mice were infected with 5 × 10^7 CFU *Shigella* by oral gavage. Two days later, small intestine was stained with DCLK1 (red), CD45 (white), Ki67 (green), and EpCAM (blue) antibodies. White arrowheads indicate $Ki67^+$ Tuft-2 cells. Triangles denote $Ki67^-$ Tuft-2 cells. Scale bar, 20 μm. Data are representative of three independent experiments.

(C) Schematic diagram of *Sh2d6*-CreERT2;*Rosa26*-iDTR-EGFP mouse construction.

(D) Experimental strategy for depleting Tuft-2 cells (upper). *Sh2d6*-CreERT2;*Rosa26*-iDTR-EGFP mice were pretreated with TAM (75 mg/kg i.p. for 3 consecutive days), followed by intraperitoneal injection with diphtheriatoxin (DT, 4 μg/kg) or PBS as control for 2 consecutive days. On day 3, small intestines were collected and stained with EGFP (green), EpCAM (red) antibodies, and DAPI (blue). Scale bar, 50 μm. Data are representative of three independent experiments.

(legend continued on next page)

CellPress

As a specific type of epithelial cells, Tuft cells harbor unique morphological and transcriptome identity. Tuft cells constitutively express some key enzymes such as Alox5, COX1, COX2, and Hpgds (Bezençon et al., 2008; Gerbe et al., 2011; O'Leary et al., 2019). Pou2f3 is an essential transcription factor (TF) for Tuft cell development (Gerbe et al., 2016). Transient receptor potential cation channel subfamily M member 5 (Trpm5) is indispensable for Tuft cell expansion (Howitt et al., 2016). Through single-cell RNA sequencing (scRNA-seq), intestinal Tuft cells are clustered into two separate subpopulations, Tuft-1 and Tuft-2 subsets (Haber et al., 2017). Tuft-1 cell signature genes are correlated with neuronal development, whereas Tuft-2 cells are related to immune response. However, it is unknown how these two subsets of Tuft cells function. Here, we identified Sh2d6 as a specific marker for Tuft-2 cells. Tuft-2 cells highly express VR Vmn2r26 that senses bacterial metabolite N-undecanoylglycine (N-C11-G), leading to prostaglandin D2 (PGD2) production to facilitate mucus secretion of goblet cells against bacterial infection.

RESULTS

Sh2d6 is a specific marker for Tuft-2 cells

Tuft cells are chemosensory cells of intestines and initiate type 2 immune responses against parasites (Gerbe et al., 2016; Howitt et al., 2016; von Moltke et al., 2016). A recent report shows that Tuft cells are classified into two subsets, Tuft-1 and Tuft-2, through scRNA-seq (Haber et al., 2017). Tuft-1 signature genes are related to neuronal development, whereas Tuft-2 signature genes are enriched for immune-related genes. Intriguingly, *Ptprc*, encoding an immune cell marker CD45, is specifically expressed in Tuft-2 cells. However, it is unclear how Tuft-2 cells function in gut immunity. To characterize Tuft-2 cells, we performed three-dimensional (3D) imaging in ileums and colons. We observed that CD45 was expressed strongly and exclusively in part of Tuft cells. We called this subpopulation Tuft-2 cells. Of note, CD45 was expressed on apical sides of Tuft-2 cells (Figure S1A). Moreover, Tuft-2 cells distributed in different regions of whole gut (Figure 1A).

To further explore the character of Tuft-2 cells, we conducted transcriptome analysis from Haber's scRNA-seq data (Haber et al., 2017). We noticed that *Sh2d6* gene was specifically expressed in Tuft-2 cells (Figures S1B–S1D). In addition, *Sh2d6* was also highly expressed in Tuft-2 cells contained tissues, including gastrointestinal tract, lung, and thymus (Figure S1C). Single-cell trajectories showed that Tuft-1 and Tuft-2 cells were two terminal mature populations and displayed distinct developmental directions (Figure S1E). To trace Tuft-2 cells, we inserted enhanced green fluorescent protein (EGFP) encoding sequence into *Sh2d6* locus to report *Sh2d6* expression for *Sh2d6*^{EGFP} reporter mice (Figure S2A). We also inserted HA tag into *Sh2d6* locus (*Sh2d6*-HA) for probing Sh2d6 expression (Figure S2B). As expected, Sh2d6-EGFP only was expressed in CD45^{+} Tuft-2 but not in CD45^{-} Tuft-1 subset (Figure 1B), indicating that *Sh2d6* is an unique reporter gene for Tuft-2 cells. We next sorted Sh2d6^{+} Tuft-2 cells from *Sh2d6*^{EGFP} mice and performed gene microarray analysis. Consistent with the previous report (Haber et al., 2017), Tuft-2 cells highly expressed *Ptprc*, *Sh2d6*, as well as other pan-Tuft marker genes, but not neuron-related genes (Figure 1C).

We also quantified frequencies of Sh2d6^{+} and Sh2d6^{-} Tuft cells of *Sh2d6*^{EGFP} mice by flow cytometry. We observed that Sh2d6^{+} Tuft-2 cells highly expressed DCLK1 and EpCAM (Figures S2C and S2D). Moreover, Sh2d6^{+} Tuft-2 cells and Sh2d6^{-} Tuft-1 cells were two separate subsets both in small intestine and colon. Sh2d6^{+} Tuft-2 cells highly expressed CD45, but Sh2d6^{-} Tuft-1 cells did not (Figures 1D and S2E). We identified that *Tppp3* was a unique gene for Tuft-1 cells (Figure S2F). We next stained intestinal tissues with antibodies against Tppp3 and Sh2d6. We observed that Tppp3 positive Tuft-1 cells did not express Sh2d6. By contrast, Sh2d6 positive Tuft-2 cells did not express Tppp3 either (Figures 1E and S2G). These data indicate that Sh2d6 is a specific marker for Tuft-2 cells, and Tppp3 is a unique marker for Tuft-1 cells.

Tuft-2 cells exert antibacterial function

Shigella is one of the most common intestinal pathogenic bacteria that causes human diarrhea. We then infected mice with *Shigella*. Under *Shigella* infection, Tuft-2 cells rapidly expanded at an early stage both in small intestines and colons (Figures 2A, S3A, and S3B), whereas Tuft-1 cell numbers had no apparent change during bacterial infection. Accordingly, Ki67 was highly expressed in some of Tuft-2 cells (Figure 2B). We next generated *Sh2d6*-CreERT2 mice (Figure S3C) and established *Sh2d6*-CreERT2;*Rosa26*-LSL-iDTR-EGFP mice (Figure 2C). With tamoxifen (TAM) and diphtheria toxin (DT) treatment, Tuft-2 cells were successfully depleted (Figure 2D), whereas Tuft-1 cells still existed (Figure S3D). To guarantee complete Tuft-2 depletion and eliminate possible newly produced Tuft-2, we performed another round of TAM plus DT treatment post *Shigella* challenge (Figure 2E). Without infection, Tuft-2 depleted mice caused little damage of intestinal integrity. However, with *Shigella* infection, Tuft-2 depleted mice showed severe damage of intestines and colons (Figure 2F). Consistently, villus epithelium was lost, and

(E) Experimental strategy for Tuft-2 cell depletion and infection with Shigella (upper). *Rosa26*-iDTR-EGFP and *Sh2d6*-CreERT2;*Rosa26*-iDTR-EGFP mice were pretreated with TAM (75 mg/kg, i.p.) and DT (4 μg/kg, i.p.) at indicated time points. Mice were orally infected with *Shigella* (5×10^7 CFU), followed by additional administration of TAM and DT. Small intestines were collected at indicated time points.

(F) Small intestine and colon of treated mice in (E) were collected on day 7. Paraffin section and H&E were performed. Scale bar, 50 μm. Data are representative of three independent experiments.

(G) Pathological scores of indicated mice in (F); n = 6 biological replicates.

(H) Colon of treated mice in (E) was collected on day 3, followed by homogenization and clonal examination of CFU; n = 6 biological replicates.

(I) Body weight changes at indicated time points of treated mice in (E); n = 6 biological replicates.

(J) Survival rates of treated mice in (E); n = 8 biological replicates.

Results are shown as means ± SEM. * $p < 0.05$, ** $p < 0.01$, NS, no significant (two-tailed Student's t test was used for [G] and [H]; unpaired test was used for [I] and [J]). Please also see Figure S3.

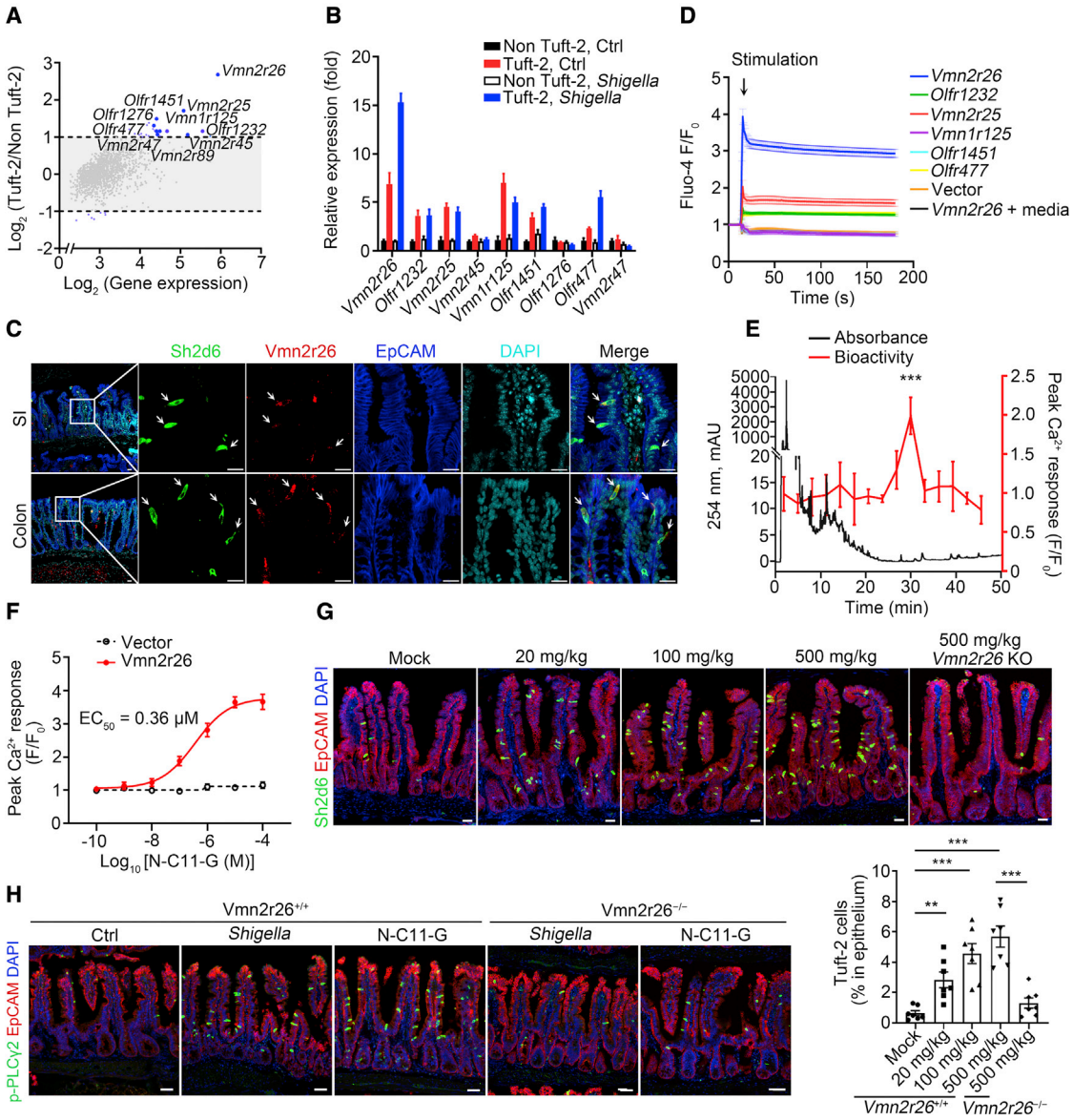

Figure 3. Vmn2r26 is highly expressed on Tuft-2 cells and recognizes *Shigella* metabolite N-C11-G

(A) Transcriptome of Tuft-2 and non-Tuft-2 epithelial cells were analyzed, and olfactory-related genes were selected. Top 10 of the most specifically and highly expressed genes are shown.

(B) Mice were infected by oral gavage of *Shigella* (5×10^7 CFU) or PBS as control. Two days post treatment, Tuft-2 and non-Tuft-2 cells were sorted and expression of indicated genes were analyzed by quantitative real-time PCR. Results were normalized to endogenous *Actb* gene; n = 3 biological replicates. Data are representative of three independent experiments.

(C) Small intestine and colon tissues were collected from *Sh2d6*-HA mice. Vmn2r26 mRNA (red) was analyzed by fluorescence *in situ* hybridization. HA tag (for Sh2d6) (green) and EpCAM (blue) were stained with indicated antibodies. Nuclei were counterstained with DAPI (cyan). Scale bar, 20 μm. Data are representative of three independent experiments.

(D) Indicated genes were overexpressed in HEK293T. Two days later, calcium probe Fluo-4 AM (2.5 μM) was loaded. Cells were stimulated with *Shigella* culture supernatants and fluorescent signals of Fluo-4 were detected with FLIPR real-time kinetic system. Related fluorescence intensity was calculated as F/F_0; n = 6 biological replicates. Data are representative of three independent experiments.

(E) Components in *Shigella* culture supernatants were separated with high performance liquid chromatography (HPLC) and sampled every 3 min. Vmn2r26 overexpressed HEK293T cells were stimulated by different fractionations and fluorescent signals of Fluo-4 were detected with FLIPR system. HPLC chromatograms (black) showing absorbance at 254 nm and red line showing peak Ca^{2+} responses of each fractionation were presented together. Data are representative of three independent experiments.

(F) Vmn2r26 and empty vector were transfected into HEK293 cells. Two days later, calcium probe Fluo-4 AM (2.5 μM) was loaded, and cells were stimulated with different doses of N-C11-G. Fluorescent signals of Fluo-4 were detected with FLIPR system. EC_{50} was calculated; n = 4 biological replicates. Data are representative of two independent experiments.

(legend continued on next page)

inflammatory leukocytes infiltrated into submucosa in intestines and colons of *Sh2d6*-CreERT2;iDTR mice (Figure 2F). In addition, *Sh2d6*-CreERT2;iDTR mice showed more severe colitis (Figure 2G), more *Shigella* bacteria load in colons (Figure 2H), and more serious weight loss (Figure 2I). All Tuft-2 depleted mice died within 9 days after *Shigella* infection (Figure 2J). Collectively, Tuft-2 cells play a critical role in gut immunity against bacterial infection.

Vmn2r26 is highly expressed on Tuft-2 cells and senses bacterial metabolite N-undecanoylglycine

Tuft cells harbor chemosensory characteristics, with their brushes of apical microvilli morphology and chemosensory signature genes, such as *Trpm5* and *Plcb2*. Recent studies show that Tuft cells share succinate receptor (SUCNR1) and T2Rs to sense various irritants of diverse lumenal substances (Luo et al., 2019; Nadjsombati et al., 2018). Through transcriptome analysis, we noticed that several olfactory-related receptor genes were highly expressed in Tuft-2 cells (Figure 3A). We chose top 10 highly expressed olfactory-related receptor genes in Tuft-2 cells and analyzed their expression under *Shigella* infection. We found that a VR gene *Vmn2r26* was highly expressed in Tuft-2 and increased over *Shigella* infection (Figure 3B). Accordingly, Vmn2r26 was mostly colocalized with Sh2d6 via fluorescence *in situ* hybridization assay (Figure 3C), indicating that Vmn2r26 is mainly expressed on Tuft-2 cells.

Since olfactory-related receptors are GPCRs, receptor activation can be assessed by a calcium indicator to detect Ca^{2+} flux. HEK293T cells were ectopically expressed with candidate olfactory-related receptors, then loaded with Ca^{2+}-sensitive dye Fluo-4 AM (Meixiong et al., 2019), followed with *Shigella* culture supernatant treatment. We found that Vmn2r26 expression caused dramatic Ca^{2+} flux in response to *Shigella* culture supernatant stimulation (Figure 3D). This result suggested that Vmn2r26 could recognize certain components of *Shigella* culture supernatants. We next wanted to identify candidate ligands in *Shigella* culture supernatants engaged with receptor Vmn2r26. We used high performance liquid chromatography (HPLC) to fractionate *Shigella* culture supernatants and challenged Vmn2r26 expressed HEK293T cells with various *Shigella* culture fractions. We observed that the fraction 10 caused remarkable Ca^{2+} flux (Figures 3E and S4A). Through liquid chromatography-tandem mass spectrometry (LC-MS/MS) assay of the fraction 10, N-C11-G was identified to be a candidate ligand (Figures S4B and S4C). We demonstrated that N-C11-G was a *Shigella* metabolite. We synthesized N-C11-G, and the binding value of half maximal effective concentration (EC_{50}) was 0.36 μM (Figure 3F).

To determine whether Tuft-2 cells can sense intestine luminal N-C11-G through Vmn2r26, we generated Vmn2r26 deficient mice (Figure S4D). We treated mice with various concentrations of N-C11-G via oral administration. We found that N-C11-G caused Tuft-2 expansion in a dose-dependent manner, whereas N-C11-G could not induce Tuft-2 cell proliferation in Vmn2r26 deficient mice (Figure 3G). Tuft-2 cell expansion reached a peak at days 4–5 (Figure S5A). Consistently, Tuft-2 cells in $Vmn2r26^{-/-}$ mice failed to expand over *Shigella* infection (Figure S5B), suggesting that Vmn2r26 is a critical receptor on Tuft-2 cells to sense *Shigella* metabolite N-C11-G.

As a type of GPCR, Vmn2r26 recognizes exogenic stimuli and transduces signals by activating phospholipase C (PLC), which catalyzes hydrolysis of PIP2 to produce 2 s messengers IP_3 and DAG (Wootten et al., 2018). We found that *Plcg2* was most highly expressed in Tuft-2 compared with other PLC family members (Figure S5C). We also observed that PLCγ2 existed in $CD45^+$ Tuft-2 cells (Figure S5D). In addition, N-C11-G treatment caused much more phosphorylation of PLCγ2. However, N-C11-G could not activate PLCγ2 phosphorylation in $Vmn2r26^{-/-}$ Tuft-2 cells (Figure 3H). *Shigella* infection displayed similar results (Figure 3H).

Since N-C11-G can initiate Tuft-2 cell expansion, we then pretreated mice with N-C11-G for 3 days, followed by *Shigella* infection. We found that N-C11-G pretreatment could protect mice against *Shigella* infection, whereas $Vmn2r26^{-/-}$ mice had no such protective effect (Figures S5E–S5H). Additionally, *Vmn2r26* deficiency caused more severe infection (Figures S5E–S5H). Collectively, Vmn2r26 is highly expressed on Tuft-2 cells and senses bacterial metabolite N-C11-G to initiate Tuft-2 cell expansion.

N-C11-G-mediated Tuft-2 cell proliferation is independent of IL-13 signaling

IL-13 promotes epithelial progenitors to give rise to Tuft and goblet cells (Gerbe et al., 2016; von Moltke et al., 2016). Vmn2r26-deficient intestinal cells still generated Tuft cells with IL-4 and IL-13 treatment. In addition, we pretreated epithelial organoids with IL-13 to induce Tuft cells, and then, IL-13 was removed from organoids culture and added N-C11-G for further stimulation. We found that Tuft-2 cells well expanded with N-C11-G challenge (Figure 4A), suggesting that N-C11-G induces Tuft-2 cell proliferation in the absence of IL-13 signaling.

We next tested whether N-C11-G engagement altered mucosal immunity. We found that gut immune cells we tested did not display significant change under N-C11-G stimulation (Figure 4B). Moreover, type 2 cytokine production had no obvious change either (Figure 4C). IL-13 signaling blockade did not disturb Tuft-2 cell expansion under N-C11-G treatment (Figure 4D). These data suggest that N-C11-G-mediated Tuft-2 cell expansion does not rely on type 2 cytokine.

Given that Tuft cells play a critical role in intestinal regeneration after tissue damage (Westphalen et al., 2014), we explored whether N-C11-G was released during tissue damage and

(G) $Vmn2r26^{+/+}$ and $Vmn2r26^{-/-}$ mice were crossed with *Sh2d6*-HA mice and treated with indicated concentrations of N-C11-G via oral administration for 3 days. Small intestines were stained with HA tag (for Sh2d6) (green) and EpCAM (red) antibodies and DAPI (blue) (upper). Percentages of Tuft-2 cells in total epithelial cells were calculated (lower). Scale bar, 20 μm. 50 crypt-villus units per mouse; n = 7 biological replicates.

(H) $Vmn2r26^{+/+}$ and $Vmn2r26^{-/-}$ mice were infected with *Shigella* (5×10^7 CFU) by orally gavage. Others were treated with N-C11-G (100 mg/kg) for 2 days. Small intestine was collected and stained with p-PLCγ2 (green) and EpCAM (red) antibodies and DAPI (blue). Scale bar, 20 μm. Data are representative of three independent experiments.

Results are shown as means ± SEM. ** $p < 0.01$, *** $p < 0.001$ (two-tailed Student's t test). Please also see Figures S4 and S5.

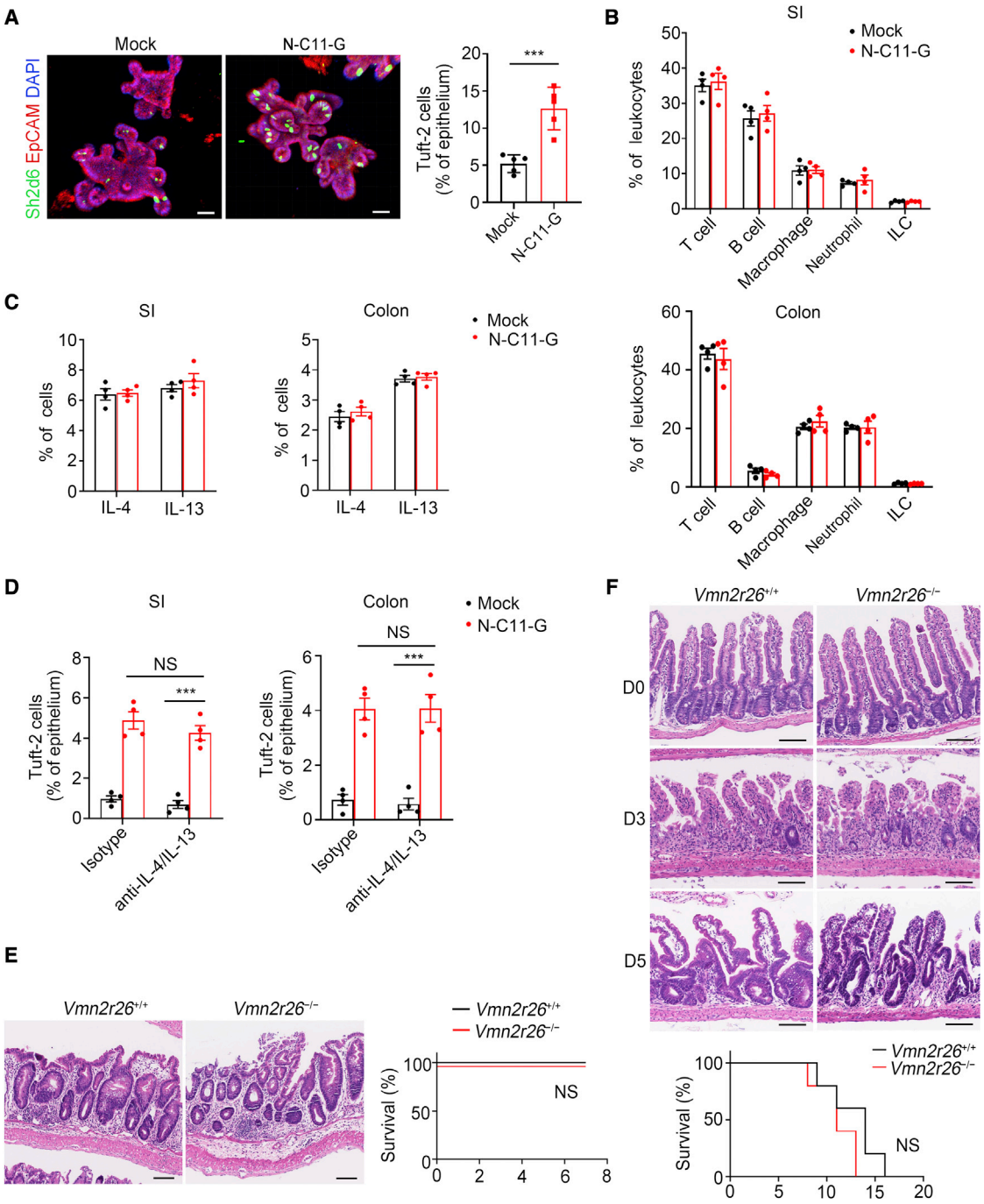

Figure 4. N-C11-G promotes Tuft-2 cell proliferation independent of IL-13 signaling

(A) Organoids were formed from intestinal crypt cells of *Sh2d6*-HA mice. In total, 400 ng/mL IL-13 were added into medium for 1 day. Then IL-13 was removed, and N-C11-G (25 μM) was added. Two days later, organoids were collected and stained with HA tag (for Sh2d6, green) and EpCAM (red) antibodies. Nuclei were counterstained with DAPI (blue). Scale bar, 50 μm. Percentages of Tuft-2 cells in epithelial cells were counted; n = 5 biological replicates. Data are representative of three independent experiments.

(B) Mice were treated with N-C11-G (100 mg/kg) for 2 days. Small intestine and colon tissues were collected and T cells ($CD3^+$), B cells ($CD19^+$), macrophages ($CD11b^+F4/80^+$), neutrophils ($CD11b^+/Gr\text{-}1^+$), and ILCs ($lineage^-CD127^+CD90^+$) were analyzed by flow cytometry. n = 4 biological replicates.

(C) Mice were treated with N-C11-G as in (B). Cells expressing IL-4 and IL-13 were analyzed by flow cytometry. n = 4 biological replicates.

(D) WT mice were treated with 20-mg/kg antibodies by tail vein injection to neutralize IL-4 and IL-13. Isotype IgG was used as control. Then mice were stimulated with N-C11-G (100 mg/kg) for 3 days. Small intestines and colons were collected and stained with HA (for Sh2d6) antibody and DAPI. Percentages of Tuft-2 cells per total epithelium were calculated; n = 4 biological replicates.

(legend continued on next page)

participated in intestinal damage repair. We then treated WT and Vmn2r26$^{-/-}$ mice with DSS or radiation to cause intestinal damage. We observed that WT and Vmn2r26$^{-/-}$ mice displayed similar intestinal tissue morphology and survival rates with treatment of DSS or radiation (Figures 4E and 4F), suggesting that intestinal tissue damage does not release N-C11-G to generate Tuft cells for tissue damage repair.

N-undecanoylglycine engagement with Vmn2r26 initiates PGD2 production in Tuft-2 cells

We next wanted to determine the molecular mechanism by which Tuft-2 cells participated in antibacterial immunity. We analyzed transcriptome of Tuft-2 cells versus other epithelial cells with gene ontology (GO) pathway enrichment analysis. Expectedly, GPCR and Ca^{2+} signaling pathways enriched in Tuft-2 cells. PG metabolic process also enriched in Tuft-2 cells (Figure 5A). PGD2 production needs several key synthases, including cytosolic phospholipase A2 (cPLA2, encoded by gene *Pla2g4a*), PG-endoperoxide synthase 1 (COX1, encoded by *Ptgs1*), PG-endoperoxide synthase 2 (COX2, encoded by *Ptgs2*), and hematopoietic PG D synthase (HPGDS, encoded by *Hpgds*) (Dennis and Norris, 2015). These key PG synthases were highly expressed in Tuft-2 cells (Figure 5B). To assess PGD2 secretion in Tuft-2 cells, we established monolayers with primary IECs (Figure S6A). With N-C11-G treatment, PGD2 was produced in monolayer cells in a dose-dependent fashion (Figure 5C). As expected, *Shigella* culture supernatant treatment showed similar results (Figure 5D). By contrast, Vmn2r26$^{-/-}$ monolayers failed to produce PGD2 over N-C11-G or *Shigella* culture supernatant treatment (Figures 5C and 5D). shRNA silencing of the key synthases disrupted PGD2 production (Figures 5E and S6B). These data suggest that Vmn2r26 is required for PGD2 production.

Given that succinate receptor SUCNR1 can sense succinate secreted by parasites (Nadjsombati et al., 2018; Schneider et al., 2018), we then silenced *Sucnr1* in monolayer cells. We observed that *Sucnr1* shRNA silencing did not affect PGD2 production, whereas *Vmn2r26* silencing abrogated PGD2 production (Figure 5F). Expectedly, *Plcg2* silencing also abolished PGD2 production (Figures 5F and S6B). Since cPLA2 activation is Ca^{2+}dependent in macrophages (von Moltke et al., 2012), we wanted to determine whether Vmn2r26-mediated PGD2 synthesis in Tuft-2 was dependent on Ca^{2+} signaling. Membrane permeable Ca^{2+} chelator (BAPTA-AM) treatment could block PGD2 production (Figure 5F), suggesting that Vmn2r26-mediated PGD2 production depends on Ca^{2+} signaling. HPGDS is a key enzyme that catalyzes the conversion of PGH2 to PGD2. We observed that HPGDS was mainly expressed in CD45^{+} Tuft-2 cells in intestines and colons (Figures 5G and S6C). Under N-C11-G challenge, phosphorylated cPLA2 (p-cPLA2) was increased in Vmn2r26$^{+/+}$ Tuft-2 cells (Figures 5H and S6D), and HPGDS was consequently highly expressed in Vmn2r26$^{+/+}$ Tuft-2 cells (Figures 5I and S6E). By contrast, Vmn2r26$^{-/-}$ Tuft-2 cells failed to activate cPLA2 phosphorylation and HPGDS expression (Figures 5H, 5I, S6D, and S6E). Taken together, N-C11-G engagement with Vmn2r26 initiates the Ca^{2+} dependent signaling pathway to produce PGD2 in Tuft-2 cells.

PGD2 facilitates mucus secretion of goblet cells to flush bacteria away from intestinal epithelia

PG is considered to play critical roles in goblet cell hyperplasia and mucus production in airway during allergy (Brightling and Brusselle, 2020). We then wanted to explore how PGD2 secreted by Tuft-2 exerts antibacterial function. We generated *Hpgds*$^{fl/fl}$ mice via CRISPR-Cas9 technology and established *Sh2d6*-CreERT2;*Hpgds*$^{fl/fl}$ mice by crossing *Sh2d6*-CreERT2 and *Hpgds*$^{fl/fl}$ mice (Figures S6F and S6G). We observed that HPGDS deletion in Tuft-2 cells dramatically diminished mucus layer thickness (Figure 6A). Colons have two mucus layers—the inner layer adheres to epithelial cells that is devoid of bacteria, whereas bacteria are present in the outer layer (Bergstrom et al., 2020; Nyström et al., 2021). We used FITC-conjugated wheat germ agglutinin (WGA), which binds to sialic acid residues known to be abundant in colonic mucin to probe mucus (Hasegawa et al., 2017), and bacteria were stained by FISH with general bacterial 16S rRNA probe EUB338 (Okumura et al., 2016). We found that HPGDS deficient mice displayed much thinner inner layer mucus and much less mucus amount (Figure 6B). These data suggest that PGD2 produced by Tuft-2 cells regulates mucus secretion. Consequently, large amounts of bacteria were distributed in close proximity in epithelial cells of *Sh2d6*-CreERT2;*Hpgds*$^{fl/fl}$ mice (Figures 6B and 6C). To further test whether PGD2 regulated mucus secretion of goblet cells, we treated colons with PGD2 or N-C11-G, followed by mucus secretion assay. We noticed that PGD2-treated goblet cells almost lacked mucus (Figures 6D and S6H), suggesting PGD2 promotes mucus secretion of goblet cells. Of note, N-C11-G stimulation also facilitated mucus release from goblet cells (Figures 6D and S6H). Expectedly, PGD2 synthase inhibitor HQL-79 treatment abrogated N-C11-G-induced mucus release from goblet cells (Figures 6D and S6H). These data suggest that PGD2 produced by Tuft-2 potentiates goblet cells to secrete mucus.

Leukotrienes are other eicosanoid lipid mediators and usually accompanied by production of PGs (Wei and Gronert, 2019). We next detected colonic mucus thickness with stimulation of PGD2 or cysteinyl leukotrienes LTC4, LTD4, and LTE4. We found that three kinds of cysteinyl leukotrienes only induced very weak mucus thickness growth compared with that of PGD2 challenge (Figure 6E). Mucus secretion helps to flush bacteria away from intestinal epithelium, which reduces bacterial load in colonic lumen and impedes pathogen invasion (Birchenough et al., 2016). We used fluorescent protein mCherry to label *Shigella* (*Shigella*^{mCherry}), followed by transanal injection into mice. We noticed that luminal *Shigella*^{mCherry} in WT mice was separated from the epithelial cell layer and quickly flashed out within 6 h (Figure 6F). By contrast, HPGDS deficiency caused *Shigella*^{mCherry} adhesion to colonic epithelia and successfully

(E) Vmn2r26$^{+/+}$ and Vmn2r26$^{-/-}$ mice were treated with DSS by drinking water containing 3% DSS. Seven days later, colons were collected and performed with H&E staining. Survival rates are shown. Data are representative of three independent experiments.
(F) Vmn2r26$^{+/+}$ and Vmn2r26$^{-/-}$ mice were treated with whole-body irradiation (12 Gy). At the indicated time points, small intestines were collected and performed with H&E staining. Survival rates are shown. Scale bar, 100 μm; n = 6 biological replicates. Data are representative of three independent experiments. Results are shown as means ± SEM. Two-tailed Student's t test was used for (A–D); unpaired test was used for (E and F). NS, not significant, *** $p < 0.001$.

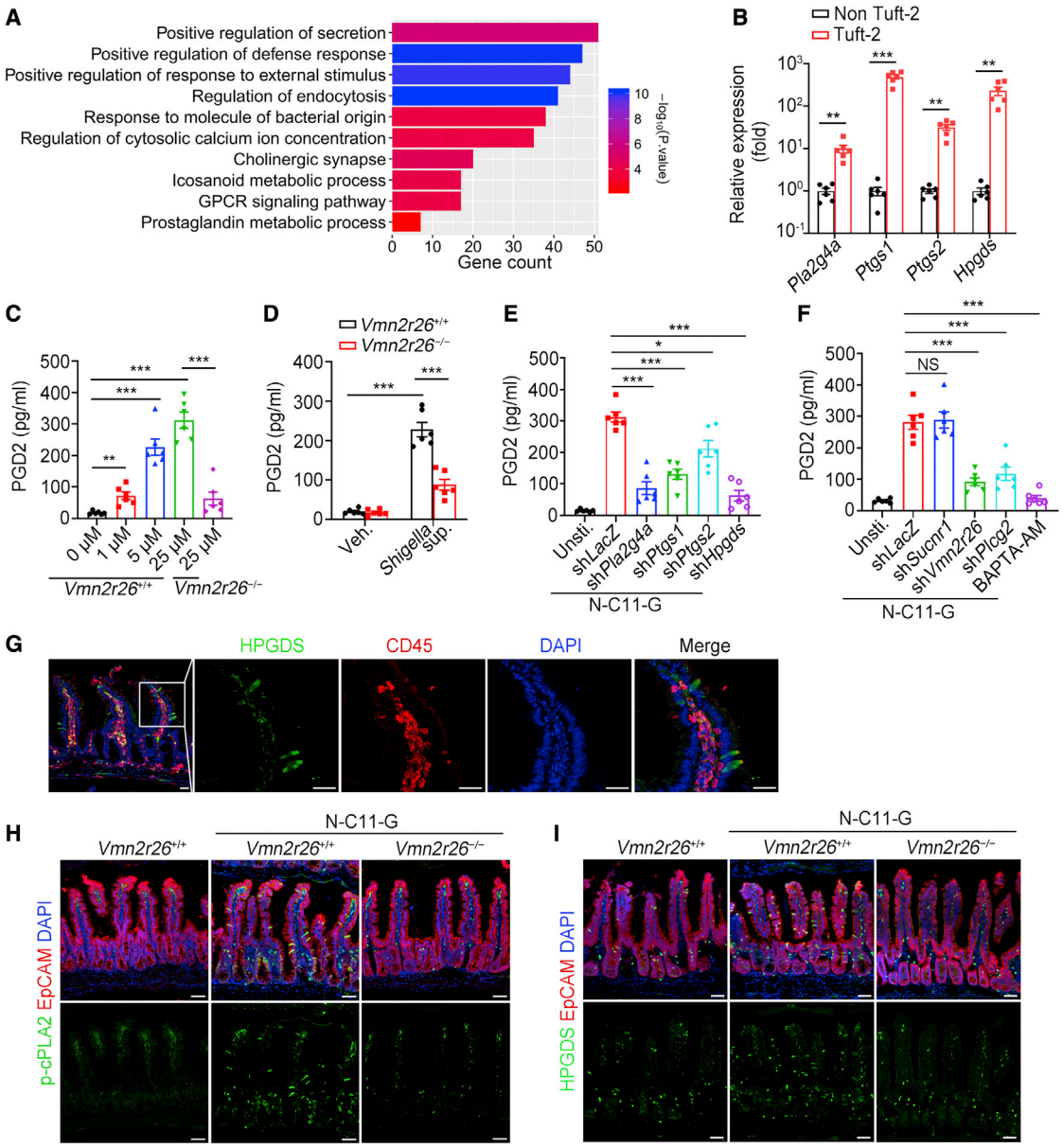

Figure 5. Engagement of Vmn2r26 with N-C11-G induces Tuft-2 cells to produce PGD2

(A) Transcriptome of Tuft-2 and non-Tuft-2 epithelial cells were analyzed. Highly expressed genes (>2-fold change) in Tuft-2 cells were selected and performed GO enrichment. GO pathways related to immune response are shown.

(B) Expressions of indicated genes in Tuft-2 cells and non-Tuft-2 epithelial cells were analyzed with qPCR. Results were normalized to the expression of endogenous *Actb* gene; n = 4 biological replicates.

(C and D) Intestinal monolayers of Vmn2r26$^{+/+}$ and Vmn2r26$^{-/-}$ mice were stimulated with indicated concentrations of N-C11-G (C) or *Shigella* culture supernatants (D) for 30 min. Culture supernatants were collected for PGD2 analysis by ELISA; n = 6 biological replicates.

(E) Intestinal organoids were infected with pLVshRNA-Puro lentivirus to silence indicated genes, followed by monolayer culture. Monolayers were treated with 25 μM N-C11-G for 30 min. Culture supernatants were collected for PGD2 analysis by ELISA; n = 6 biological replicates.

(F) Intestinal monolayers were treated with 25 μM N-C11-G with indicated conditions, and PGD2 production was detected by ELISA 30 min post treatment. *Sucnr1*, *Vmn2r26*, or *Plcg2* were silenced with pLVshRNA-Puro lentivirus. Ca^{2+} signaling was blocked with a cell-permeable Ca^{2+} chelator BAPTA-AM (10 μM); n = 6 biological replicates.

(G) Small intestines were stained with HPGDS (green) and CD45 (red) antibodies and DAPI (blue). Data are representative of three independent experiments.

(H and I) Vmn2r26$^{+/+}$ and Vmn2r26$^{-/-}$ mice were treated with N-C11-G (100 mg/kg) for 2 days. Small intestine was collected and stained with p-cPLA2 (H) or HPGDS (I) (green) and EpCAM (red) antibodies. Nuclei were counterstained with DAPI (blue). Data are representative of three independent experiments.

Results are shown as means ± SEM. * $p < 0.05$ and ** $p < 0.01$, *** $p < 0.001$; NS, no significant (two-tailed Student's t test). Please also see Figure S6.

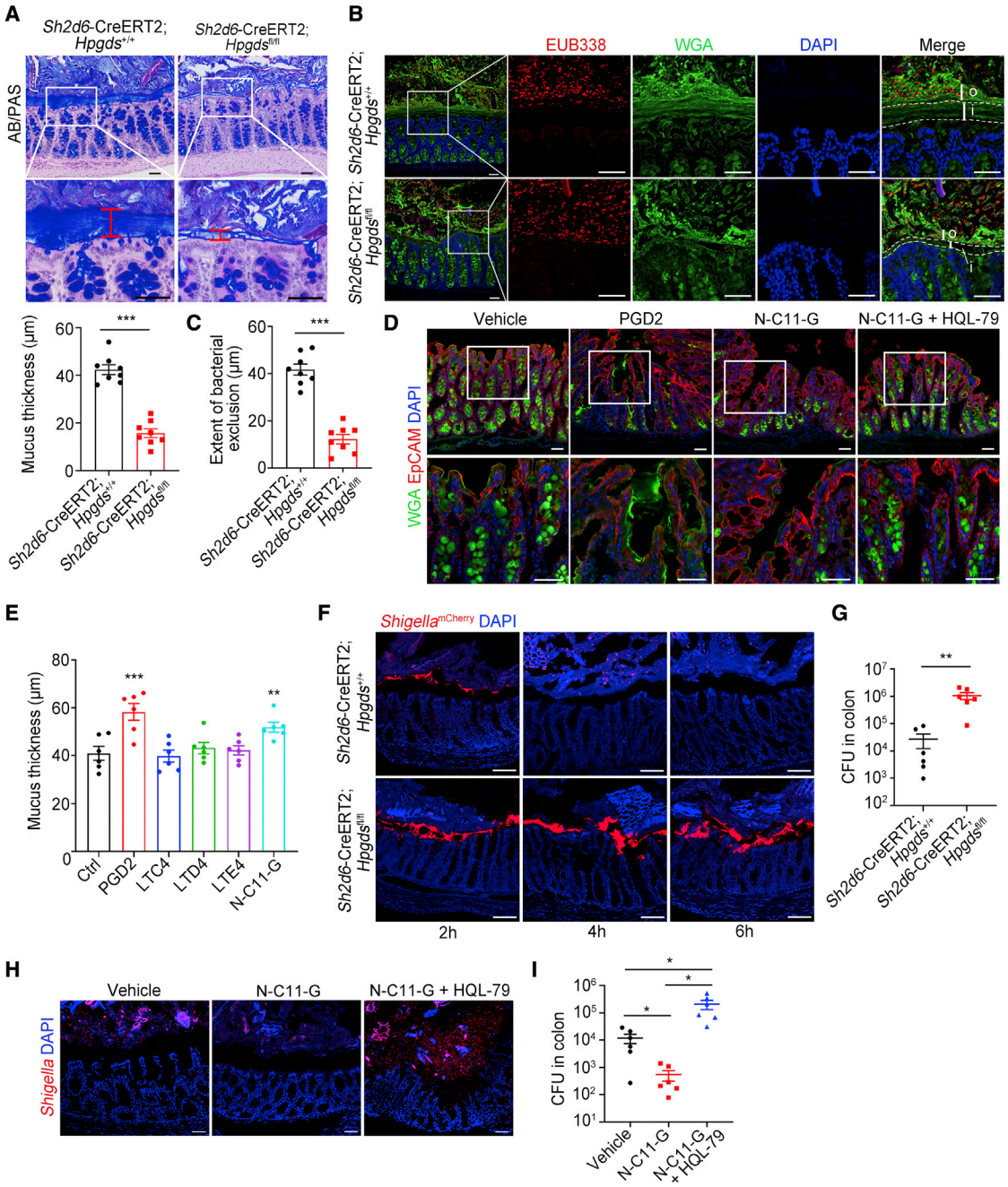

Figure 6. PGD2 produced by Tuft-2 cells facilitates mucus secretion to flush *Shigella* away from epithelial cells

(A) *Sh2d6*-CreERT2;*Hpgds*$^{+/+}$ and *Sh2d6*-CreERT2;*Hpgds*$^{fl/fl}$ mice were treated with TAM (75 mg/kg, i.p.) for 7 days, and colon was collected. Paraffin sections of colon were stained with AB/PAS (periodic acid-Schiff and Alcian blue) (upper). Mucus thickness was measured (lower). Data are representative of three independent experiments.

(B) Mice were treated as in (A). Colons were fixed with Carnoy's solution. Bacteria were stained by FISH using EUB338 probe (red). Mucus was stained with FITC-conjugated WGA (green). Nuclei were counterstained with DAPI (blue). Data are representative of three independent experiments.

(C) Extent of bacterial exclusion of colon tissues from mice in (B); n = 8 biological replicates.

(D) Mice were stimulated with PGD2 (100 nM), N-C11-G (25 μM), or N-C11-G (25 μM) plus HPGDS inhibitor HQL-79 (10 μM), respectively, by rectal injection. Thirty min later, colons were collected and stained with FITC-conjugated WGA (green), EpCAM (red) antibody, and DAPI (blue). Data are representative of three independent experiments.

(E) Mice were stimulated with PGD2 (100 nM), LTC4 (100 nM), LTD4 (100 nM), LTE4 (100 nM), or N-C11-G (25 μM), respectively, by rectal injection. Thirty min later, colons were collected and sliced directly without washing. Mucous thickness was measured; n = 6 biological replicates.

(legend continued on next page)

colonized in colonic tissues (Figure 6F). Consequently, bacteria load in colonic tissues of *Sh2d6*-CreERT2;*Hpgds*$^{fl/fl}$ mice was much higher than that of *Sh2d6*-CreERT2;*Hpgds*$^{+/+}$ mice (Figure 6G). These data indicate that PGD2 produced by Tuft-2 cells is necessary to prevent *Shigella* infection. Finally, N-C11-G pretreatment was able to impede *Shigella*^{mCherry} colonization in colonic tissues of WT mice. However, PGD2 synthase inhibitor HQL-79 abolished N-C11-G-mediated *Shigella*^{mCherry} clearance (Figures 6H and 6I). Collectively, PGD2 produced by Tuft-2 cells facilitates mucus secretion of goblet cells to flush bacteria away from intestinal epithelia, leading to bacterial clearance.

Vmn2r26 signaling promotes expansion of Tuft-2 cells via SpiB expression

Through transcriptome analysis of Sh2d6^{+} Tuft-2 cells and other epithelium, we picked the top 10 TFs highly expressed in Tuft-2 cells (Figure 7A). We silenced each of these 10 TFs and performed organoids-based Tuft-2 development assay. We found that shRNA silencing of *Pou2f3*, *Gfi1b*, and *Spib* significantly suppressed Tuft-2 development (Figures 7B and S7A). *Pou2f3* and *Gfi1b* were reported to be expressed in Tuft cells and regulate Tuft cell development (Schneider et al., 2019). Ets TF SpiB (encoded by *Spib*) plays an important role in the development of B cells, plasmacytoid dendritic cells (pDCs), and intestinal M cells (Kishikawa et al., 2017; Macal et al., 2018; Willis et al., 2017). However, it is unclear how SpiB regulates Tuft-2 cell development and function. We noticed that *Spib* expression was remarkably increased over N-C11-G challenge (Figures 7C and S7B). However, Vmn2r26$^{-/-}$ Tuft-2 cells failed to augment *Spib* expression with N-C11-G stimulation (Figure 7C). In addition, Plcγ2 inhibitor 3-nitrocoumarin blocked *Spib* expression (Figure 7C). These data indicate that Vmn2r26-Plcγ2 signaling axis enhances *Spib* expression and promotes Tuft-2 cell proliferation.

We next generated *Spib*$^{fl/fl}$ mice via CRISPR-Cas9 technology and established *Lgr5*-CreERT2-EGFP;*Spib*$^{fl/fl}$ mice (Figures S7C and S7D). We found that SpiB deletion in Lgr5^{+} intestinal stem cells (ISCs) reduced Tuft-2 cell numbers compared with those of WT mice (Figure 7D). We also established *Sh2d6*-CreERT2;*Spib*$^{fl/fl}$ mice to delete *Spib* in Tuft-2 cells (Figure S7E). We observed that SpiB deletion in Tuft-2 cells also reduced Tuft-2 cell numbers (Figure 7E). By contrast, CD45^{-} Tuft-1 cells still existed (Figure S7F). In addition, SpiB deletion failed to promote Tuft-2 cell expansion under N-C11-G stimulation (Figure 7F). These data indicate that SpiB is required for the proliferation of Tuft-2 cells over bacterial infection.

We next measured mucus thickness in *Sh2d6*-CreERT2;*Spib*$^{fl/fl}$ mice. As expected, SpiB deficiency in Tuft-2 cells caused mucus layer thinning (Figure S7G). Tuft-2 cell depletion in *Sh2d6*-CreERT2;iDTR mice obtained similar observations (Figure S7H). We infected *Sh2d6*-CreERT2;*Spib*$^{fl/fl}$ mice with *Shigella* and noticed that SpiB deletion in Tuft-2 cells caused much more severe inflammation and intestinal damage (Figure 7G). Consistently, bacteria load was much higher in colonic tissues of *Sh2d6*-CreERT2;*Spib*$^{fl/fl}$ mice (Figure 7H). In addition, *Sh2d6*-CreERT2;*Spib*$^{fl/fl}$ mice showed more body weight loss and higher death rates after *Shigella* infection (Figures 7I and 7J). Altogether, Vmn2r26 signaling promotes development and expansion of Tuft-2 cells via SpiB expression, which is required for bacterial clearance.

DISCUSSION

Succinate receptor SUCNR1 is highly expressed in intestinal Tuft cells, which binds to succinate to initiate type 2 response for protists colonization and alterations in microbiota (Lei et al., 2018; Nadjsombati et al., 2018; Schneider et al., 2018). The downstream cation channel Trpm5 is required for the hyperplasia and activation of Tuft cells. Unlike Trpm5$^{-/-}$ mice, *Sucnr1*$^{-/-}$ mice have no remarkable defect in Tuft cell hyperplasia and worm clearance (Nadjsombati et al., 2018). These data suggest that the intestine may contain other sensing pathways to induce protective responses against helminths (Nadjsombati et al., 2018). The vomeronasal organ detects pheromones and other semiochemicals via VRs, which are a special class of olfactory receptors (Isogai et al., 2011). In addition, peptide ligands of major histocompatibility complex (MHC) molecules also engage VRs, which can influence social behavior (Leinders-Zufall et al., 2004). Besides nose, olfactory receptors are expressed on other tissues. For example, olfactory receptor Olfr558 is expressed on enterochromaffin cells, acting as a metabolite sensor to trigger Ca^{2+} signaling (Bellono et al., 2017). Herein, we show that Tuft-2 cells also express some olfactory receptors, especially highly expressing Vmn2r26. Under bacterial infection, Vmn2r26 senses bacterial metabolite N-C11-G to activate PLCγ2 and Ca^{2+} signaling in Tuft-2 cells, facilitating cell expansion and PGD2 production.

PGs, containing PGD2, PGE2, PGI2, and PGF2α mainly generated *in vivo*, play critical roles in the induction of inflammatory response and tumorigenesis (Roulis et al., 2020). PG generation is very low in normal tissues but increases immediately in acute inflammation, prior to the recruitment of immune cells. The cyclooxygenases (COX1 and COX2) convert arachidonic acid first into PGG2 and then to PGH2. Unstable endoperoxide PGH2 can be further catalyzed to thromboxane A2 (TXA2), PGI2, PGE2, PGF2, and PGD2 (Dennis and Norris, 2015). PG D synthases (PGDS), such as lipocalin PG D synthase (LPGDS) and HPGDS, convert PGH2 to PGD2 (Dennis and Norris, 2015). We show that Tuft cells highly express cPLA2 and HPGDS under N-C11-G

(F) *Sh2d6*-CreERT2;*Hpgds*$^{+/+}$ and *Sh2d6*-CreERT2;*Hpgds*$^{fl/fl}$ mice were treated with TAM (75 mg/kg, i.p.) for 7 days. *Shigella*^{mCherry} (10^9 CFU) was inoculated into mice by rectal injection. Colons were collected at indicated time points and fixed with 4% PFA. Colon sections were counterstained with DAPI. Data are representative of three independent experiments.

(G) Colons were collected from mice as in (F) 12 h after inoculation. CFU of *Shigella* in colon was analyzed; n = 6 biological replicates.

(H and I) Mice were treated with N-C11-G (25 μM) or N-C11-G (25 μM) plus HPGDS inhibitor HQL-79 (10 μM) by rectal injection. Six h later, colons were collected and stained with DAPI (H). Colons were collected 12 h after inoculation of *Shigella*. CFU of *Shigella* were analyzed (I); n = 6 biological replicates.

Results are shown as means ± SEM. * $p < 0.05$ and ** $p < 0.01$, *** $p < 0.001$ (two-tailed Student's t test). For data in (A), (C), and (E), thickness of mucus layer at 30 different sites of each sample was measured, and averaged thickness was calculated. Please also see Figure S6.

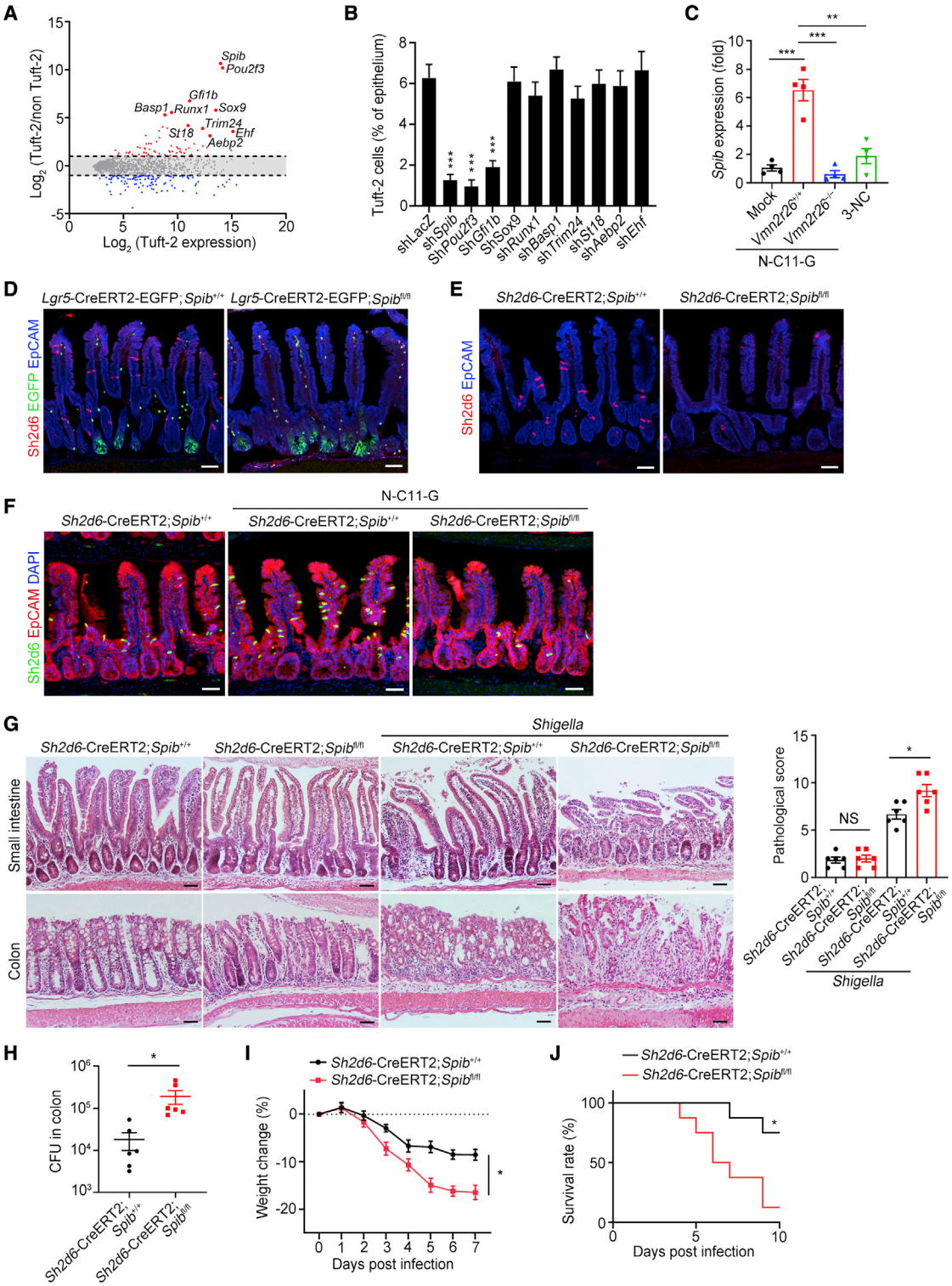

Figure 7. SpiB is required for Vmn2r26-mediated Tuft-2 cell expansion

(A) Transcriptomes of Tuft-2 cells and non-Tuft-2 epithelial cells were analyzed. Expression of transcription factors are shown, and top 10 of most specifically and highly expressed TFs in Tuft-2 cells are marked.

(B) Intestinal organoids derived from *Sh2d6*^{EGFP} mice were cultured, and top 10 selected TFs were respectively silenced with pLVshRNA-Puro lentivirus. In total, 1 μg/mL puromycin, IL-4 (400 ng/mL), and IL-13 (400 ng/mL) were added into culture media. Percentages of Tuft-2 cells per total epithelium were calculated; n = 10 biological replicates.

(legend continued on next page)

stimulation. Moreover, engagement of Vmn2r26 with N-C11-G initiates large amounts of PGD2 production. Goblet cells as a type of IECs are specialized for the synthesis and secretion of mucus, flashing bacteria away upon infection. PGE_2 induces mucus secretion in mouse small intestine and colon (Ermund et al., 2013). Deletion of HPGDS in Tuft-2 cells results in insufficient mucus secretion, leading to severe infection. It still needs further investigation about how PGD2 induces mucus secretion by goblet cells.

Like other epithelial lineages, Tuft cells derive from ISCs, both under steady conditions as well as in response to injury (Beumer and Clevers, 2021; von Moltke et al., 2016). However, it is unclear how Tuft cells develop and expand upon bacterial infection. Among Ets family members, SpiB, SpiC, and PU.1 show closely related overall structures and Ets domains, forming a Spi-B related subfamily. These SpiB subfamily members activate the promoters of downstream target genes in cooperation with interferon regulatory factor (IRF) family members to mediate immune responses (Care et al., 2014). SpiB is exclusively expressed in mature B cells, T-cell progenitors, and pDCs (Willis et al., 2017). SpiB is also involved in M cell differentiation in the gut (Kishikawa et al., 2017). In this study, we conclude that SpiB is required for the development and expansion of Tuft-2 cells upon bacterial infection. In summary, we define Tuft-2 cells as an innate immune cell in the gut that sense bacterial metabolite N-C11-G via VR Vmn2r26, whose engagement initiates PGD2 production and SpiB expression. PGD2 then facilitates mucus secretion of goblet cells to promote antimicrobial immunity, and SpiB induces the development and expansion of Tuft-2 cells under bacterial challenge.

Limitations of the study

The intestinal epithelium is a highly structured tissue. Resent studies showed that the most common cell type enterocytes and the rare cell types, such as goblet and Tuft cells, exhibit zonated expression programs along the crypt-villus axis (Manco et al., 2021; Moor et al., 2018). Manco et al showed that Tuft-1 specific genes preferably express toward the bottom of the villus, whereas Tuft-2 specific transcripts are zonated toward the villus tip (Manco et al., 2021). We have not identified specific marker genes for Tuft-1 subset to generate Tuft-1 marker gene-driven creERT2 mice. Due to this limitation, we could not define Tuft-1 function but only speculate based on their transcriptional characteristics. Given that Tuft-1 cells express a neuronal development gene signature, Tuft-1 cells appear to be more poised for neuromodulation. Tuft-1 cells also express taste transduction-related genes, such as Plcb and Gnat3, as well as choline acetyltransferase (ChAT), which suggest that Tuft-1 subset might be involved in the input signal transduction from gut environment to neurons. Of note, Vmn2r26 may enhance maturation of Tuft cells by increasing SpiB expression, which contributes to the phenotype of Tuft cell expansion during an early phase of bacteria infection. It still needs to further investigate how Tuft cells undergo differentiation and maturation during the process of bacteria infection.

STAR★METHODS

Detailed methods are provided in the online version of this paper and include the following:

- KEY RESOURCES TABLE
- RESOURCE AVAILABILITY
  - Lead contact
  - Materials availability
  - Data and code availability
- EXPERIMENTAL MODEL AND SUBJECT DETAILS
  - Mice
- METHOD DETAILS
  - Immunofluorescence imaging
  - 3D fluorescence imaging
  - Single-cell tissue preparation and cell sorting
  - Bacterial strain
  - Mouse treatment and infection
  - Pathological score and histologic analysis
  - Quantitative real-time PCR
  - Crypt isolation and organoid culture
  - shRNA gene silencing
  - ELISA assay
  - Calcium imaging

(C) Vmn2r26$^{+/+}$;*Sh2d6*^{EGFP} and Vmn2r26$^{-/-}$;*Sh2d6*^{EGFP} mice were stimulated with N-C11-G (100 mg/kg) for 2 days. Mice were treated with Plcγ2 inhibitor 3-nitrocoumarin (3-NC, 30 μM, i.p.). Two days later, Tuft-2 cells were sorted, and *Spib* expression was analyzed by qPCR; n = 4 biological replicates.
(D) *Lgr5*-CreERT2-EGFP;*Spib*$^{+/+}$;*Sh2d6*-HA and *Lgr5*-CreERT2-EGFP;*Spib*$^{fl/fl}$;*Sh2d6*-HA mice were treated with TAM (75 mg/kg, i.p.) for 7 days. Small intestines were collected at day 7 and stained with HA (for Sh2d6) (red) and EpCAM (blue). ISCs were marked by EGFP (green). Scale bar, 50 μm. Data are representative of three independent experiments.
(E) *Sh2d6*-CreERT2;*Spib*$^{+/+}$;*Sh2d6*-HA and *Sh2d6*-CreERT2;*Spib*$^{fl/fl}$;*Sh2d6*-HA mice were treated with TAM (75 mg/kg, i.p.) for 7 days. Small intestines were collected at day 7 and stained with HA tag (for Sh2d6) (red) and EpCAM (blue) antibodies. Scale bar, 50 μm. Data are representative of three independent experiments.
(F) *Sh2d6*-CreERT2;*Spib*$^{+/+}$;*Sh2d6*-HA and *Sh2d6*-CreERT2;*Spib*$^{fl/fl}$;*Sh2d6*-HA mice were treated with TAM (75 mg/kg, i.p.) for 7 days, and on the 5th day, mice were treated with 100 mg/kg N-C11-G for 2 days. Small intestines were collected and stained with HA tag (for Sh2d6) (green) and EpCAM (red) antibodies. Nuclei were stained with DAPI (blue).
(G) *Sh2d6*-CreERT2;*Spib*$^{+/+}$ and *Sh2d6*-CreERT2;*Spib*$^{fl/fl}$ mice were treated with TAM (75 mg/kg, i.p.) for 7 days, and on the 5th day, mice were orally infected with *Shigella* (5×10^7 CFU). Small intestines and colons were collected 7 days after infection and stained with H&E (left). Scale bar, 50 μm. Pathological scores were calculated (right); n = 6 biological replicates.
(H) Colon of treated mice as in (G) was collected 3 days after infection, followed by homogenization and clonal examination of CFU; n = 6 biological replicates.
(I) Body weight changes of mice in (G) at indicated time points; n = 7 biological replicates.
(J) Survival rates of mice in (G) at the indicated time points; n = 8 biological replicates.
Results are shown as means ± SEM. * $p < 0.05$ and ** $p < 0.01$, *** $p < 0.001$ (two-tailed Student's t test was used for [B], [C], [G], and [H]; unpaired test was used for [I] and [J]).
Please also see Figure S7.

- Fluorescence in situ hybridization (FISH)
- Liquid chromatography–mass spectrometry
- Mucus thickness measurement
- Microarray assay and bioinformatic analysis

- QUANTIFICATION AND STATISTICAL ANALYSIS

SUPPLEMENTAL INFORMATION

Supplemental information can be found online at https://doi.org/10.1016/j.immuni.2022.03.001.

ACKNOWLEDGMENTS

We thank Yihui Xu for technical support. We thank Xiang Shi, Xing Gao, Zixin Zhao, Ming Hao, Jiajia Hou and Xin Wen for animal procedures. We thank Zhimin Wang for data analysis. We thank Yan Teng and Yun Feng for imaging technical support. We thank Ya Wang for technical support. We also thank Jing Li (Cnkingbio Company Ltd, Beijing, China) for technical support. This work was supported by the National Key R&D Program of China (2020YFA0803501, 2019YFA0508501, 2021YFF0702802), National Natural Science Foundation of China (31930036, 81921003, 92042302, 32070533, 91940305, 81772646, 82130088), Strategic Priority Research Programs of the Chinese Academy of Sciences (XDB19030203), Biological Resources Program of Chinese Academy of Sciences (KFJ-BRP-017), the Young Elite Scientist Sponsorship Program by CAST (2018QNRC001), the Beijing Natural Science Foundation (5222023), and the Postdoctoral grant (2020M680712).

AUTHOR CONTRIBUTIONS

Z.X. designed and performed experiments, analyzed data, and wrote the paper; X.Z. generated genetic mice and analyzed data; J.G. and Y.X. performed experiments; R.W., C.L., and D.F. performed some experiments and crossed mice; X.Q. and Y.D. analyzed some data; Y.T. generated animal models and analyzed data; Z.F. initiated the study, organized, designed, and wrote the paper.

DECLARATION OF INTERESTS

The authors declare no competing interests.

Received: May 17, 2021
Revised: October 8, 2021
Accepted: March 1, 2022
Published: March 22, 2022

REFERENCES

Bellono, N.W., Bayrer, J.R., Leitch, D.B., Castro, J., Zhang, C., O'Donnell, T.A., Brierley, S.M., Ingraham, H.A., and Julius, D. (2017). Enterochromaffin cells are gut chemosensors that couple to sensory neural pathways. Cell *170*, 185.e16–198.e16.

Bergstrom, K., Shan, X., Casero, D., Batushansky, A., Lagishetty, V., Jacobs, J.P., Hoover, C., Kondo, Y., Shao, B., Gao, L., et al. (2020). Proximal colon-derived O-glycosylated mucus encapsulates and modulates the microbiota. Science *370*, 467–472.

Beumer, J., and Clevers, H. (2021). Cell fate specification and differentiation in the adult mammalian intestine. Nat. Rev. Mol. Cell Biol. *22*, 39–53.

Bezençon, C., Fürholz, A., Raymond, F., Mansourian, R., Métairon, S., Le Coutre, J., and Damak, S. (2008). Murine intestinal cells expressing Trpm5 are mostly brush cells and express markers of neuronal and inflammatory cells. J. Comp. Neurol. *509*, 514–525.

Birchenough, G.M., Nyström, E.E., Johansson, M.E., and Hansson, G.C. (2016). A sentinel goblet cell guards the colonic crypt by triggering Nlrp6-dependent Muc2 secretion. Science *352*, 1535–1542.

Brightling, C.E., and Brusselle, G. (2020). The impact of the prostaglandin D_2 receptor 2 and its downstream effects on the pathophysiology of asthma. Allergy *75*, 761–768.

Bufe, B., Teuchert, Y., Schmid, A., Pyrski, M., Pérez-Gómez, A., Eisenbeis, J., Timm, T., Ishii, T., Lochnit, G., Bischoff, M., et al. (2019). Bacterial MgrB peptide activates chemoreceptor Fpr3 in mouse accessory olfactory system and drives avoidance behaviour. Nat. Commun. *10*, 4889.

Caers, J., Peymen, K., Suetens, N., Temmerman, L., Janssen, T., Schoofs, L., and Beets, I. (2014). Characterization of G protein-coupled receptors by a fluorescence-based calcium mobilization assay. J. Vis. Exp. *89*, e51516.

Care, M.A., Cocco, M., Laye, J.P., Barnes, N., Huang, Y., Wang, M., Barrans, S., Du, M., Jack, A., Westhead, D.R., et al. (2014). SPIB and BATF provide alternate determinants of IRF4 occupancy in diffuse large B-cell lymphoma linked to disease heterogeneity. Nucleic Acids Res. *42*, 7591–7610.

Dalton, R.P., and Lomvardas, S. (2015). Chemosensory receptor specificity and regulation. Annu. Rev. Neurosci. *38*, 331–349.

Dennis, E.A., and Norris, P.C. (2015). Eicosanoid storm in infection and inflammation. Nat. Rev. Immunol. *15*, 511–523.

Desai, P., Janova, H., White, J.P., Reynoso, G.V., Hickman, H.D., Baldridge, M.T., Urban, J.F., Jr., Stappenbeck, T.S., Thackray, L.B., and Diamond, M.S. (2021). Enteric helminth coinfection enhances host susceptibility to neurotropic flaviviruses via a tuft cell-IL-4 receptor signaling axis. Cell *184*, 1214.e16–1231.e16.

Erben, U., Loddenkemper, C., Doerfel, K., Spieckermann, S., Haller, D., Heimesaat, M.M., Zeitz, M., Siegmund, B., and Kühl, A.A. (2014). A guide to histomorphological evaluation of intestinal inflammation in mouse models. Int. J. Clin. Exp. Pathol. *7*, 4557–4576.

Ermund, A., Schütte, A., Johansson, M.E., Gustafsson, J.K., and Hansson, G.C. (2013). Studies of mucus in mouse stomach, small intestine, and colon. I. Gastrointestinal mucus layers have different properties depending on location as well as over the Peyer's patches. Am. J. Physiol. Gastrointest. Liver Physiol. *305*, G341–G347.

Gerbe, F., Sidot, E., Smyth, D.J., Ohmoto, M., Matsumoto, I., Dardalhon, V., Cesses, P., Garnier, L., Pouzolles, M., Brulin, B., et al. (2016). Intestinal epithelial tuft cells initiate type 2 mucosal immunity to helminth parasites. Nature *529*, 226–230.

Gerbe, F., van Es, J.H., Makrini, L., Brulin, B., Mellitzer, G., Robine, S., Romagnolo, B., Shroyer, N.F., Bourgaux, J.F., Pignodel, C., et al. (2011). Distinct ATOH1 and Neurog3 requirements define tuft cells as a new secretory cell type in the intestinal epithelium. J. Cell Biol. *192*, 767–780.

Haber, A.L., Biton, M., Rogel, N., Herbst, R.H., Shekhar, K., Smillie, C., Burgin, G., Delorey, T.M., Howitt, M.R., Katz, Y., et al. (2017). A single-cell survey of the small intestinal epithelium. Nature *551*, 333–339.

Hasegawa, Y., Mark Welch, J.L., Rossetti, B.J., and Borisy, G.G. (2017). Preservation of three-dimensional spatial structure in the gut microbiome. PLoS One *12*, e0188257.

Howitt, M.R., Lavoie, S., Michaud, M., Blum, A.M., Tran, S.V., Weinstock, J.V., Gallini, C.A., Redding, K., Margolskee, R.F., Osborne, L.C., et al. (2016). Tuft cells, taste-chemosensory cells, orchestrate parasite type 2 immunity in the gut. Science *351*, 1329–1333.

Isogai, Y., Si, S., Pont-Lezica, L., Tan, T., Kapoor, V., Murthy, V.N., and Dulac, C. (2011). Molecular organization of vomeronasal chemoreception. Nature *478*, 241–245.

Ke, M.T., Fujimoto, S., and Imai, T. (2013). SeeDB: a simple and morphology-preserving optical clearing agent for neuronal circuit reconstruction. Nat. Neurosci. *16*, 1154–1161.

Kishikawa, S., Sato, S., Kaneto, S., Uchino, S., Kohsaka, S., Nakamura, S., and Kiyono, H. (2017). Allograft inflammatory factor 1 is a regulator of transcytosis in M cells. Nat. Commun. *8*, 14509.

Lei, W., Ren, W., Ohmoto, M., Urban, J.F., Jr., Matsumoto, I., Margolskee, R.F., and Jiang, P. (2018). Activation of intestinal tuft cell-expressed Sucnr1 triggers type 2 immunity in the mouse small intestine. Proc. Natl. Acad. Sci. USA *115*, 5552–5557.

Leinders-Zufall, T., Brennan, P., Widmayer, P., S, P.C., Maul-Pavicic, A., Jäger, M., Li, X.H., Breer, H., Zufall, F., and Boehm, T. (2004). MHC class I peptides as chemosensory signals in the vomeronasal organ. Science *306*, 1033–1037.

Luo, X.-C., Chen, Z.-H., Xue, J.-B., Zhao, D.-X., Lu, C., Li, Y.-H., Li, S.-M., Du, Y.-W., Liu, Q., Wang, P., et al. (2019). Infection by the parasitic helminth Trichinella spiralis activates a Tas2r-mediated signaling pathway in intestinal tuft cells. Proc. Natl. Acad. Sci. USA *116*, 5564–5569.

Macal, M., Jo, Y., Dallari, S., Chang, A.Y., Dai, J., Swaminathan, S., Wehrens, E.J., Fitzgerald-Bocarsly, P., and Zúñiga, E.I. (2018). Self-renewal and toll-like receptor signaling sustain exhausted plasmacytoid dendritic cells during chronic viral infection. Immunity *48*, 730.e5–744.e5.

Manco, R., Averbukh, I., Porat, Z., Bahar Halpern, K., Amit, I., and Itzkovitz, S. (2021). Clump sequencing exposes the spatial expression programs of intestinal secretory cells. Nat. Commun. *12*, 3074.

McGinty, J.W., Ting, H.A., Billipp, T.E., Nadjsombati, M.S., Khan, D.M., Barrett, N.A., Liang, H.E., Matsumoto, I., and von Moltke, J. (2020). Tuft-cell-derived leukotrienes drive rapid anti-helminth immunity in the small intestine but are dispensable for anti-protist immunity. Immunity *52*, 528.e7–541.e7.

Meixiong, J., Vasavda, C., Snyder, S.H., and Dong, X. (2019). MRGPRX4 is a G protein-coupled receptor activated by bile acids that may contribute to cholestatic pruritus. Proc. Natl. Acad. Sci. USA *116*, 10525–10530.

Miller, C.N., Proekt, I., von Moltke, J., Wells, K.L., Rajpurkar, A.R., Wang, H., Rattay, K., Khan, I.S., Metzger, T.C., Pollack, J.L., et al. (2018). Thymic tuft cells promote an IL-4-enriched medulla and shape thymocyte development. Nature *559*, 627–631.

Montoro, D.T., Haber, A.L., Biton, M., Vinarsky, V., Lin, B., Birket, S.E., Yuan, F., Chen, S., Leung, H.M., Villoria, J., et al. (2018). A revised airway epithelial hierarchy includes CFTR-expressing ionocytes. Nature *560*, 319–324.

Moor, A.E., Harnik, Y., Ben-Moshe, S., Massasa, E.E., Rozenberg, M., Eilam, R., Bahar Halpern, K., and Itzkovitz, S. (2018). Spatial reconstruction of single enterocytes uncovers broad zonation along the intestinal villus axis. Cell *175*, 1156.e15–1167.e15.

Nadjsombati, M.S., McGinty, J.W., Lyons-Cohen, M.R., Jaffe, J.B., DiPeso, L., Schneider, C., Miller, C.N., Pollack, J.L., Nagana Gowda, G.A., Fontana, M.F., et al. (2018). Detection of succinate by intestinal tuft cells triggers a Type 2 innate immune circuit. Immunity *49*, 33.e7–41.e7.

Nyström, E.E.L., Martinez-Abad, B., Arike, L., Birchenough, G.M.H., Nonnecke, E.B., Castillo, P.A., Svensson, F., Bevins, C.L., Hansson, G.C., and Johansson, M.E.V. (2021). An intercrypt subpopulation of goblet cells is essential for colonic mucus barrier function. Science *372*, eabb1590.

Okumura, R., Kurakawa, T., Nakano, T., Kayama, H., Kinoshita, M., Motooka, D., Gotoh, K., Kimura, T., Kamiyama, N., Kusu, T., et al. (2016). Lypd8 promotes the segregation of flagellated microbiota and colonic epithelia. Nature *532*, 117–121.

O'Leary, C.E., Schneider, C., and Locksley, R.M. (2019). Tuft cells-systemically dispersed sensory epithelia integrating immune and neural circuitry. Annu. Rev. Immunol. *37*, 47–72.

Rivière, S., Challet, L., Fluegge, D., Spehr, M., and Rodriguez, I. (2009). Formyl peptide receptor-like proteins are a novel family of vomeronasal chemosensors. Nature *459*, 574–577.

Roulis, M., Kaklamanos, A., Schernthanner, M., Bielecki, P., Zhao, J., Kaffe, E., Frommelt, L.S., Qu, R., Knapp, M.S., Henriques, A., et al. (2020). Paracrine orchestration of intestinal tumorigenesis by a mesenchymal niche. Nature *580*, 524–529.

Schneider, C., O'Leary, C.E., and Locksley, R.M. (2019). Regulation of immune responses by tuft cells. Nat. Rev. Immunol. *19*, 584–593.

Schneider, C., O'Leary, C.E., von Moltke, J., Liang, H.E., Ang, Q.Y., Turnbaugh, P.J., Radhakrishnan, S., Pellizzon, M., Ma, A., and Locksley, R.M. (2018). A metabolite-triggered tuft cell-ILC2 circuit drives small intestinal remodeling. Cell *174*, 271–284.e14.

von Moltke, J., Ji, M., Liang, H.E., and Locksley, R.M. (2016). Tuft-cell-derived IL-25 regulates an intestinal ILC2-epithelial response circuit. Nature *529*, 221–225.

von Moltke, J., Trinidad, N.J., Moayeri, M., Kintzer, A.F., Wang, S.B., van Rooijen, N., Brown, C.R., Krantz, B.A., Leppla, S.H., Gronert, K., and Vance, R.E. (2012). Rapid induction of inflammatory lipid mediators by the inflammasome in vivo. Nature *490*, 107–111.

Wei, J., and Gronert, K. (2019). Eicosanoid and specialized proresolving mediator regulation of lymphoid cells. Trends Biochem. Sci. *44*, 214–225.

Weiß, E., and Kretschmer, D. (2018). Formyl-peptide receptors in infection, inflammation, and cancer. Trends Immunol. *39*, 815–829.

Westphalen, C.B., Asfaha, S., Hayakawa, Y., Takemoto, Y., Lukin, D.J., Nuber, A.H., Brandtner, A., Setlik, W., Remotti, H., Muley, A., et al. (2014). Long-lived intestinal tuft cells serve as colon cancer-initiating cells. J. Clin. Invest. *124*, 1283–1295.

Willis, S.N., Tellier, J., Liao, Y., Trezise, S., Light, A., O'Donnell, K., Garrett-Sinha, L.A., Shi, W., Tarlinton, D.M., and Nutt, S.L. (2017). Environmental sensing by mature B cells is controlled by the transcription factors PU.1 and SpiB. Nat. Commun. *8*, 1426.

Wootten, D., Christopoulos, A., Marti-Solano, M., Babu, M.M., and Sexton, P.M. (2018). Mechanisms of signalling and biased agonism in G protein-coupled receptors. Nat. Rev. Mol. Cell Biol. *19*, 638–653.

Xiong, Z., Xia, P., Zhu, X., Geng, J., Wang, S., Ye, B., Qin, X., Qu, Y., He, L., Fan, D., et al. (2020). Glutamylation of deubiquitinase BAP1 controls self-renewal of hematopoietic stem cells and hematopoiesis. J. Exp. Med. *217*, e20190974.

Zhu, P., Zhu, X., Wu, J., He, L., Lu, T., Wang, Y., Liu, B., Ye, B., Sun, L., Fan, D., et al. (2019). IL-13 secreted by ILC2s promotes the self-renewal of intestinal stem cells through circular RNA circPan3. Nat. Immunol. *20*, 183–194.

Zhuang, H., and Matsunami, H. (2008). Evaluating cell-surface expression and measuring activation of mammalian odorant receptors in heterologous cells. Nat. Protoc. *3*, 1402–1413.

STAR★METHODS

KEY RESOURCES TABLE

REAGENT or RESOURCE	SOURCE	IDENTIFIER
Antibodies		
DCLK1 (IF, 1: 500; FC, 1:200)	Proteintech	Cat#21699-1-AP; RRID:AB_10859251
HA Tag (IF, 1:200)	Proteintech	Cat#51064-2-AP; RRID:AB_11042321
HPGDS (IF, 1:200)	Proteintech	Cat#22522-1-AP; RRID:AB_2879115
Tppp3 (IF, 1:100)	Proteintech	Cat#15057-1-AP; RRID:AB_2878105
CD45 (30-F11) (IF, 1:500)	eBioscience	Cat#14-0451-82; RRID:AB_467251
CD45, APC conjugated (HI30) (FC, 1:100)	eBioscience	Cat#17-0459-42; RRID:AB_10667894
Ki67, FITC conjugated (SolA15) (IF, 1:300)	eBioscience	Cat#11-5698-80; RRID:AB_11151689
EpCAM, PE conjugated (1B7) (IF, 1:300; FC, 1:100)	eBioscience	Cat#12-9326-41; RRID:AB_11039407
EpCAM, Alexa Fluor 647 conjugated (G8.8) (IF, 1:300; FC, 1:100)	BioLegend	Cat#118212; RRID:AB_1134101
CD170 (Siglec-F), PE conjugated (QA20A11) (FC, 1:100)	BioLegend	Cat#164103; RRID:AB_2894437
SpiB (IF, 1:500; WB, 1:1000)	R&D Systerms	Cat#AF7204; RRID:AB_10995033
GFP Tag (IF, 1:200)	Proteintech	Cat#50430-2-AP; RRID:AB_11042881
β-actin (2D4H5) (WB, 1:2000)	Proteintech	Cat#66009-1-Ig; RRID:AB_2687938
Phospho-PLCγ2 (Tyr1217) (IF, 1:200)	Cell Signaling Technology	Cat#3871; RRID:AB_2299548
Trpm5 (WB, 1:1000)	Proteintech	Cat#18027-1-AP; RRID:AB_2287825
Phosphor-cPLA2 (Ser505) (IF, 1:200)	Immunoway	Cat#YP0868; RRID:AB_2895531
Pou2f3 (WB, 1:1000)	Bioss	Cat#bs-21046R; RRID:AB_2895533
IL-4 (30340)	R&D Systerms	Cat#MAB404; RRID:AB_2128960
IL-13 (38213)	R&D Systerms	Cat# MAB413; RRID:AB_2124171
Goat anti-Rabbit IgG (H+L), Alexa Fluor 488 conjugated (IF, 1:800)	eBioscience	Cat#A-11034; RRID:AB_2576217
Goat anti-Rabbit IgG (H+L), Alexa Fluor 594 conjugated (IF, 1:800)	eBioscience	Cat#A-11037; RRID:AB_2534095
Goat anti-Rat IgG (H+L), Alexa Fluor 594 conjugated (IF, 1:800)	eBioscience	Cat#A-21209; RRID:AB_2535795
Donkey anti-Sheep IgG (H+L), Alexa Fluor 594 conjugated (IF, 1:800)	eBioscience	Cat#A-11016; RRID:AB_2534083
Bacterial and virus strains		
Shigella flexneri	BeNa Culture Collection, China	Cat#BNCC173289
Salmonella (S.) Typhimurium	Institute of Microbiology, Chinese Academy of Sciences, China	Cat#1.1194
Chemicals, peptides, and recombinant proteins		
Recombinant Murine IL-13	PeproTech	Cat#210-13
Recombinant Murine IL-4	PeproTech	Cat#214-14
Recombinant Murine R-Spondin-1	PeproTech	Cat#315-32
Recombinant Murine EGF	PeproTech	Cat#315-09
Recombinant Murine Noggin	PeproTech	Cat#250-38
Recombinant Murine Wnt-3a	PeproTech	Cat#315-20
N-acetylcysteine	Sigma Aldrich	Cat#1009005
Matrigel matrix	Corning	Cat#356234
Type I collagenase	ThermoFisher	Cat#17018029
Y-27632	MedChemExpress	Cat#HY-10071
SB431542	MedChemExpress	Cat#HY-10431

(*Continued on next page*)

Continued		
REAGENT or RESOURCE	SOURCE	IDENTIFIER
DAPI	Sigma Aldrich	Cat#D8417
Prostaglandin D_2	Cayman Chemical	Cat#12010
DNase I	Sigma Aldrich	Cat#D4513
Succinic acid	Sigma Aldrich	Cat#S9512
FITC conjugated WGA lectin	GeneTex	Cat#GTX01502
D(−)-fructose	Sigma Aldrich	Cat#F3510
α-thioglycerol	Sigma Aldrich	Cat#M6145
Paraformaldehyde	Sigma Aldrich	Cat#P6148
TRIzol	ThermoFisher	Cat#15596026
Lipofectamine 3000 Transfection Reagent	ThermoFisher	Cat#L3000015
N-undecanoylglycine	This paper	N/A
Critical commercial assays		
FoxP3 Transcription Factor Staining Kit	ThermoFisher	Cat#00-5523-00
Prostaglandin D2 ELISA Kit	Cayman Chemical	Cat# 512031
IntestiCult Organoid Growth Medium (Mouse)	STEMCELL Technologies	Cat#06005
Alexa Fluor 488 Conjugation Kit	Abcam	Cat#ab236553
Alexa Fluor 594 Conjugation Kit	Abcam	Cat#ab269822
RNAprep Pure Micro Kit	TIANGEN	Cat#DP420
Deposited data		
Expression profiling of Tuft and Tuft-2 cells	This paper	GEO: GSE184675
Experimental models: Organisms/strains		
Mouse: C57BL/6J	Jackson Laboratory	Cat#000664
Mouse: *Lgr5*-EGFP-CreERT2	Nanjing University, China	N/A
Mouse: *Rosa26*-iDTR-EGFP	Biocytogen Pharmaceuticals, China	N/A
Mouse: *Rosa26*-EYFP	Shanghai Research Center For Model Organisms, China	Cat#SJ-006148
Mouse: B6.*Sh2d6*-CreERT2	This paper	N/A
Mouse: B6.*Sh2d6*-EGFP	This paper	N/A
Mouse: B6.*Sh2d6*-HA	This paper	N/A
Mouse: B6.*Hpgds*$^{flox/flox}$	This paper	N/A
Mouse: B6.*Spib*$^{flox/flox}$	This paper	N/A
Mouse: B6.*Vmn2r26*$^{-/-}$	This paper	N/A
Mouse: B6.*Pou2f3*$^{-/-}$	This paper	N/A
Mouse: B6.*Trpm5*$^{-/-}$	This paper	N/A
Oligonucleotides		
sgRNA sequences for mouse strain building	Table S1	N/A
Sequences of primers used for genotyping	Table S2	N/A
Sequences of primers used in real-time PCR and genotyping	Table S3	N/A
Sequences for shRNAs	Table S4	N/A
Recombinant DNA		
pLVshRNA-Puro	This paper	N/A
pLVshRNA-EGFP(2A)Puro	This paper	N/A
pLVX-IRES-Puro	This paper	N/A
psPAX2	Addgene	Cat#12260
pMD2.G	Addgene	Cat#12259
pBBR1MCS-2	Addgene	Cat#85168
pcDNA4/myc-His B Mammalian Expression Vectors	ThermoFisher	Cat#V86320

(*Continued on next page*)

Continued

REAGENT or RESOURCE	SOURCE	IDENTIFIER
Software and algorithms		
GraphPad Prism 8	GraphPad Software	https://www.graphpad.com/scientific-software/prism/
FlowJo 10.5.4	Tree Star	https://www.flowjo.com/
Imaris 9.0	Bitplane Imaris	https://imaris.oxinst.com/
NIS-Elements Imaging Software	Nikon	https://www.microscope.healthcare.nikon.com/products/software/nis-elements/
Other		
BD FACS Aria III	BD Biosciences	N/A
Nikon Confocal A1R+	Nikon	N/A
Opera Phenix high content screening system	PerkinElmer	N/A
FLIPR Penta High-Throughput Cellular Screening System	Molecular Devices	N/A

RESOURCE AVAILABILITY

Lead contact

Further information and requests for resources and reagents should be directed to and will be fulfilled by the lead contact, Zusen Fan (fanz@moon.ibp.ac.cn).

Materials availability

The materials in this study are available from the lead contact upon reasonable request.

Data and code availability

- Gene expression microarray data have been deposited at GEO and are publicly available as of the date of publication. Accession numbers are listed in the key resources table. Original western blot images have been deposited at Mendeley and are publicly available as of the date of publication. Microscopy data reported in this paper will be shared by the lead contact upon request.
- This paper does not report original codes.
- Any additional information required to reanalyze the data reported in this paper is available from the lead contact upon request. Microarray data have been deposited in the Gene Expression Omnibus (GEO) under accession number GSE184675.

EXPERIMENTAL MODEL AND SUBJECT DETAILS

Mice

Generation of *Sh2d6*-P2A-CreERT2, *Sh2d6*-P2A-EGFP, *Sh2d6*-HA, *Hpgds*$^{fl/fl}$, *Spib*$^{fl/fl}$ genetically targeted mice and Vmn2r26$^{-/-}$, Pou2f3$^{-/-}$, Trpm5$^{-/-}$ mice were based on the methods described before (Xiong et al., 2020). In brief, vector pST1374-NLS-flag-linker-Cas9 (Addgene plasmid #44758) expressing Cas9 and pUC57-sgRNA (Addgene plasmid #51132) expressing sgRNAs (Table S1) for target genes were constructed. Donor templates of P2A-CreERT2, P2A-EGFP, HA, LoxP sequences combined with homology arms were cloned into pLSODN-1. LsODNs were prepared using an LsODN Preparation Kit (Biodynamics Laboratory, Tokyo, Japan) according to the manufacturer's protocol. Mixtures of Cas9 mRNA (100 ng/μl), sgRNA (50 ng/μl) and donor templates (20 ng/μl) were microinjected into the cytoplasm of C57BL/6 fertilized eggs, followed by transferring to the uterus of pseudo-pregnant ICR females, from which viable founder mice were obtained. Genotyping of mouse tools were performed by indicated primers (Table S2) and verified by DNA sequencing. 6 to 12-wk-old mice were used for mouse experiments. All the mice are C57BL/6 background and maintained under specific pathogen-free conditions. Animal use and protocols were approved by the Institutional Animal Care and Use Committees of Institute of Biophysics, Chinese Academy of Sciences.

METHOD DETAILS

Immunofluorescence imaging

Mouse intestine and colon were excised and rinsed in pre-cold 1 x PBS. Then samples were coiled into a 'Swiss roll' and fixed with 4% paraformaldehyde (PFA) (Sigma) at room temperature (RT) for 2 hours, followed with dehydration in 30% sucrose at 4°C overnight. Then samples were embedded in OCT compound (Tissue-Tek) and stored at −80°C before sectioning (10 μm) on a Cryostat

(Leica). For immunofluorescence staining, sections were permeabilized in PBS containing 1% Triton X-100 for 30 min at RT, followed with blocking in 10% BSA for 30 min at 37°C. Primary antibodies were diluted with PBS containing 1% BSA and sections were incubated with primary antibodies on a shaker at 4°C overnight. Then sections were washed for 3 times with PBST (0.05% Tween-20 in PBS), 5 min each time, and then were incubated with secondary antibodies and DAPI for 1 h at RT. Sections were washed for 3 times with PBST. All of imaging for Sh2d6 in this work was accomplished by staining HA tag antibody, using *Sh2d6*-HA mice. After staining, sections were mounted with Fluormount G (Southern Biotech) and examined on a Nikon laser scanning confocal microscope. Images were analysed with Imaris 9 software.

3D fluorescence imaging

Imunofluorescence and three-dimensional fluorescence imaging method was derived from SeeDB (Ke et al., 2013). Mouse intestine and colon were collected and rinsed in pre-cold PBS and fixed with 4% PFA at RT for 2 h. Then intestine and colon were cut as ring shape and were washed with 1% Triton X-100 in PBS for three times (30 min each). Samples were permeabilized and blocked in permeabilizing solution (0.1% Tween-20, 0.5% TritonX-100, 0.1% Deoxycholate, 0.1% NP40, 10% BSA in PBS) at 4°C for 1 day with gentle shaking. Primary antibodies were diluted with blocking buffer (0.5 TritonX-100, 3% BSA in PBS) and samples were incubated for 2 days on a shaker at 4°C, followed with washing in washing buffer (1% TritonX-100 in PBS) for 4 times (30 min, 1 hour, 6 hours and overnight) on a shaker at 4°C. Secondary antibodies were diluted with blocking buffer and incubated samples for 1 day on a shaker at 4°C, and then samples were washed in washing buffer for 4 times (30 min, 1 h, 6 h and overnight) on a shaker at 4°C. Samples were post-fixed in 4% PFA at 4°C for 30 min. Then immunofluorescence stained samples were incubated successively in 20%, 40%, 60%, 80%, 100% (w/v) fructose solution respectively for 12 h and then incubated in SeeDB buffer, 80.2% (w/w) fructose with 0.5% (v/v) α-thioglycerol for 24 h at RT. Cleared samples were imaged using confocal scanning (Nikon) or Opera Phenix high content screening system (PerkinElmer). Z-stacks projections were compiled using Imaris 9 software.

Single-cell tissue preparation and cell sorting

Small intestines and colons were collected and tissues were opened and rinsed with pre-cold PBS to remove intestinal contents. Tissues were further rinsed and vigorously vortexed to remove mucous layer for 3 times. Then tissues were cut into 2 cm sections and incubated at 37°C with gently shaking (100 r/m) in 15ml HBSS (Ca^{2+}/Mg^{2+}-free) supplemented with 10mM HEPES (VWR Life Science), 5mM EDTA (VWR), 5mM dithiothreitol (DTT, Sigma-Aldrich) and 5% fetal calf serum (Biological Industries), followed with vortex thoroughly to release epithelial cells. This process was repeated for 3-4 times until supernatant was clean. Supernatants were pooled and passed through a 70 μm filter. Cells were washed with PBS and incubated with diluted indicated antibodies in PBS + 3% FBS on ice for 30 min. DAPI was stained for 10 min on ice. Then cells were washed twice and analyzed and sorted with BD Aria III flow cytometer. Samples were FSC-A/SSC-A gated to exclude debris, and FSC-W/FSC-A and SSC-W/SSC-A gated to select single cells. $DAPI^-$ were gated to exclude died cells. For $Sh2d6^{EGFP}$ mice, $EGFP^+EpCAM^+Siglec\text{-}F^+$ cells were sorted as $Sh2d6^+$ Tuft-2 cells, $EGFP^-EpCAM^+Siglec\text{-}F^+$ cells were sorted as $Sh2d6^-$ Tuft cells and $EGFP^-EpCAM^+$ cells were sorted as non-Tuft-2 epithelial cells. For wild type mice, $Siglec\text{-}F^+EpCAM^+CD45^+$ cells were sorted as Tuft-2 cells. Results were analyzed with FlowJo 10.

Bacterial strain

Shigella flexneri (BNCC173289) was purchased from BNBio company (Beijing, China). *Shigella* strain was cultured aerobically on a shaker (200 r/m) at 37°C in Tryptic Soy (TS) broth (Aoboxing, Beijing, China) or incubated on TS agar plates with 0.1% Congo Red (Sigma-Aldrich). *Salmonella (S.) Typhimurium* was from Institute of Microbiology, Chinese Academy of Sciences. For $Shigella^{mCherry}$ construction, mCherry was cloned into pBBR1MCS-2 vector and vector was then transfected into *Shigella* via electransfection. Briefly, *Shigella* was aerobically cultured at 37 °C temperature on shaker (220 r/m) overnight and 3ml bacteria solution was centrifuged at 4 °C for 10 min at 3,000 g. Discard the supernatant, and bacterial pellet was resuspended with 5ml ice-cold sterile ddH2O and centrifuged. Repeat wash with 5 ml ice-cold sterile H2O containing 10% glycerin for three times and finally resuspended the bacterial pellet thoroughly in 40 μl ice-cold sterile H_2O containing 10% glycerin. 1μg of plasmid DNA was added in to 40 μl bacterial suspension and mixture was transfered into a pre-cold, sterile 0.2 cm gap cuvette. Insert the cuvette into MicroPulser electroporator (BIO-RAD) and electroporated at 1.8 kV, 25 μF for 5 ms. The cell suspension was quickly recovered by resuspending into 1 ml TS broth and incubated at 37°C for 30 min. Then bacteria were plated onto TS agar plates with kanamycin. Plates were incubated at 37°C for 12 h and mCherry fluorescence of *Shigella* clones were checked with fluorescence microscope (Nikon).

Mouse treatment and infection

We established the bacterial infection models with the standard procedure. In detail, 8∼12 week-old mice were deprived of food and water for 4 hours and then were gavaged with 20 mg streptomycin sulfate in 200 μl PBS. 24 hours later, mice were again deprived of food and water for 4 hours, and then were gavaged with 5×10^7 CFUs of *Shigella* or 2×10^7 CFUs of *Salmonella*. For oral gavage, 200 μl reagents were given through oral gavage with lavage needle (size #9, bend). For rectal administration, mice were anesthetized with 1.8% isoflurane, followed by rectal injection of 200 μl reagents through a flexible catheter. Catheter was inserted into anus with 4.5 cm depth, and reagents were injected slowly to avoid overflow. Then mice were kept upside down for 3 min. For N-C11-G treatment, N-C11-G was dissolved in sterile water. 20% DMSO was added and samples were incubated at 60 °C water bath for dissolution. 20% DMSO was used as control. Mice were deprived of food and water for 4 hours and then were gavaged with N-C11-G. Mice were with indicated concentration of N-C11-G once a day.

Pathological score and histologic analysis

Mouse colons were cut open longitudinally and washed with pre-cold PBS, and then were fixed in 4% PFA fixative for 8 h at RT. Fixed tissues were washed for twice and moved to 70% ethanol for storage. Tissues were transferred sequentially to various concentrations of alcohols for dehydration and then embedded in paraffin, followed by sectioning and staining with hematoxylin and eosin (H&E) according to standard laboratory procedures. The following histological parameters were evaluated (Erben et al., 2014): leukocyte infiltration, epithelial injury, submucosal oedema and the numbers of goblet cells were the main index that measured. Leukocyte infiltration was analyzed as follows: 0, absent leukocyte infiltration; 1, mild infiltration; 2, moderate infiltration; 3, severe infiltration. Epithelial injury was scored as follows: 0, normal villus structure; 1, mild epithelium loss; 2, moderate epithelium loss; 3, severe epithelium loss; Submucosal oedema was scored as follows: 0, no oedema; 1, <50% of the submucosal area and was <100 μm wide; 2, 50–80% of the submucosal area and was <200 μm wide; 3, >80% of the submucosal area and was >200 μm wide. The average number of goblet cells was counted and scored as follows: 0, >40 goblet cells per visual field; 1, 26–40 goblet cells per visual field; 2, 16–25 goblet cells per visual field; 3, 0–15 goblet cells per visual field.

Quantitative real-time PCR

Cell populations were isolated by flow cytometry. Total RNAs were extracted with RNAprep Pure Micro Kit or TRIzol according to the manufacturer's protocol. Then cDNA was synthesized with the M-MLV reverse transcriptase (Promega, Madison, USA). mRNA transcripts were analyzed with ABI 7300 qPCR system using indicated primer pairs (Table S3). Relative expressions were calculated and normalized to endogenous *Actb* expression.

Crypt isolation and organoid culture

Small intestinal crypt isolation and organoid culture were described with modifications described below (Zhu et al., 2019). Briefly, small intestines were washed with ice-cold PBS through a 20 ml syringe, then were opened longitudinally and washed with ice-cold PBS by vigorous shaking. Villi were removed by carefully scraping with a sterile glass slides. Tissue was cut as 5 mm fragments, followed with incubation in collagenase solution (DMEM/F12 medium, containing 0.1% type I collagenase, 100 units/ml penicillin, 0.1 mg/ml streptomycin and 10 mM HEPES). Every 5 min, the samples were pipetted vigorously by a 1 ml pipette and the separation of the crypts was checked with a microscope, until more than 50% of crypts were separated from tissue fragments (about 25 min). Then the samples were filtered through a 70 μm cell strainer and centrifugated with 60g for 5 min. Discard the supernatant and the precipitant was resuspend with 200 μl pre-warmed complete organoid media. Crypts were mixed with Matrigel (Corning) and plated at 400-500 crypts per well in a prewarmed 24-well plate. After incubation at 37°C for 5 minutes for matrigel solidification, 500 μl complete organoid medium was carefully added into each well. Complete organoid medium was purchased from STEMCELL Technologies (IntestiCult organoid growth medium) or composed of Dulbecco's modified Eagle's medium/F12 medium (Invitrogen) supplemented with 2 mM L-Glutamine, 10mM HEPES, 100 units/ml Penicillin, 1,000 μg/ml Streptomycin, 1 × N2 (Invitrogen), 1 × B27 (Invitrogen), 1 mM N-acetylcysteine (NAC, Sigma-Aldrich), 500 ng/ml R-Spondin-1 (PeproTech), 50 ng/ml EGF (PeproTech), and 50 ng/ml Noggin. Medium was replaced every 2 days and organoids were analyzed 1 week later. To get enough Tuft-2 cells, 400 ng/ml IL-4 and 400 ng/ml IL-13 (PeproTech) were added into complete organoid medium. Tuft-2 cells were identified as $EGFP^{+}$ (organoids from $Sh2d6^{EGFP}$ mice) or $CD45^{+}$. For passaging and maintenance of organoids, the basement matrix dome with medium was broken using 1 ml pipetman tip and transferred to 1.5 ml tubes. Organoids were mechanically disrupted through pipetting (3-5×) with 1 ml syringe needle, until no whole organoids were visible. Cells were centrifuged 900 g for 5 min and pellets were resuspended with Matrigel for following culture. Cultures were split in 1:2 to 1:6 ratios depending on the number of organoids per dome.

shRNA gene silencing

Silencing of indicated genes was performed by short hairpin RNA as before. shRNAs of indicated genes were designed on online RNAi designer (Merck or Thermo Fisher Scientific). 3-4 shRNAs of each target gene were selected and cloned into pLVshRNA-EGFP(2A)Puro or pLVshRNA-Puro lentivirus vector (Table S4). For lentivirus packaging and concentration, 293T HEK cells were cultured in DMEM + 10% FBS on 10 cm dishes. When cells were 80–90% confluent, 6 μg pLVshRNA-EGFP(2A)Puro plasmid, 4.5 μg packaging plasmid psPAX2 and 1.5 μg envelope plasmid pMD2.G were mixed and transfected into 293T cells by using Lipofectamine 3000 reagent. Media was changed 6 h after transfection and Cells were cultured at 37°C for 2 days. Supernatants from dishes were collected and pooled, and then filtered through a 0.45 μm filter. Supernatants containing virus particles were ultracentrifuged at 25,000 rpm (82,700 g) for 2 h at 4°C for viral concentration. Then pellets were resuspended with complete organoid media at 4°C overnight. Virus were made as 20-μl aliquots and stored at –80°C. For gene silencing in organoid cells, organoids were cultured for 7 days. Organoids were broken as described in organoid passaging step. Then cells were resuspended with 500 μl complete organoid media and mixed with lentivirus solution adding 6 μg/ml polybrene (Sigma-Aldrich) and transferred into 24-well plates for centrifugation at 32°C, 600 x g, for 1 h. Cells were cultured at 37°C for 6 h. Then cells were centrifuged to remove virus and resuspended with Matrigel for organoid culture. 3 days later, EGFP of organoids was detected with fluorescence microscope and 1 μg/ml puromycin was added into the media for selection. Organoids were passaged and maintained and gene silencing efficiency was analyzed by real-time qPCR (Table S3).

ELISA assay

Intestinal monolayer cultures were generated for enzyme linked immunosorbent assay (ELISA) experiments. Organoids were derived from WT or $Vmn2r26^{-/-}$ mice. 12-well transwell inserts were coated by adding 250 μl of a 1:30 Matrigel at 37°C for 2 h and then the

excess Matrigel solution was removed. Organoids were collected and broken by pipetting with 1ml syringe needle and centrifuged 900 g for 5 min. Pellets were resuspended with monolayer culture medium (complete organoid media without NAC supplemented with 10 μM Y-27632 and 10 μM SB431542 and then were added to the precoated wells (100 μl/well). 400 μl monolayer culture medium was added in the well. Every 2 days, medium was changed using complete organoid medium without NAC and Y-27632. To get enough Tuft-2 cells, 400 ng/ml IL-4 and 400 ng/ml IL-13 were added into the medium. Monolayers should be ready for experimental use 10 days later. Since Tuft cells were initially very few in primary monolayers, we added IL-13 and IL-4 to induce Tuft cell proliferation. To exclude the effect of IL-13 and IL-4 on PGD2 production, we changed fresh culture medium without IL13 and IL-4 for 12 hours before N-C11-G treatment. For ELISA analysis of PGD2, stimulations were added into the monolayers and incubated for 30 minutes at 37°C. Supernatants were collected and used to perform ELISA using the prostaglandin D2 ELISA kit (Cayman Chemical) or acetylcholine ELISA kits (Novus Biologicals) following manufacturer's instructions.

Calcium imaging

GPCR activation was measured by a fluorescence-based calcium mobilization assay. Indicated murine receptors and other genes were cloned into pCDNA4 plasmid for overexpression. A shorter form of receptor-transporting protein 1 (RTP1S) was co-transfected to support the robust cell-surface and functional of receptors (Zhuang and Matsunami, 2008). Promiscuous murine Gα15 and human Gα16 were co-transfected to transduce the signaling and induce calcium release (Caers et al., 2014). When 293T HEK cells were 80–90% confluent, culture medium was changed with fresh DMEM + 10% FBS medium and cells were transfected indicated aforementioned plasmid with Lipofectamine 3000. 6 h later, medium was changed and cells were cultured for 24 h at 37°C. The transfected cells were collected and seeded in fibronectin (Sigma-Aldrich) coated 96-well plates, and then cells were incubated for 16 h. Cells were washed with wash buffer (1× HBSS with $Ca2^{+}/Mg^{2+}$, 10 mM HEPES, 0.1% BSA, pH 7.4). To load calcium probe, cells were incubated with wash buffer supplemented with 2.5 mM Fluo-4 AM (Invitrogen), 0.05% pluronic-F127 (Sigma-Aldrich), 1 mM probenecid (MedChemExpress) at 37°C for 30 min, followed with washing and then incubated for a further 30 minutes. Cells were washed again and ready for test. Calcium mobilization was analyzed with high throughput cellular screening system (FLIPR Tetra) or confocal. For FLIPR assay, cell plates and ligand plates were transferred to the FLIPR instrument and calcium signals were analyzed according to the instrument manual. Parameters were as follows: read time interval, 1 s; number of reads before dispense, 10; total number of reads, 190. For calcium imaging with confocal, fluorescence images were collected at 1 frames per second with on Nikon confocal and analyzed with NIS Elements AR software. Fluorescence/background (R/R0) was quantified over time.

Fluorescence in situ hybridization (FISH)

FISH staining of all bacteria in colon was performed as described before (Okumura et al., 2016). Colon tissues from indicated mice were collected without washing and fixed in methanol–Carnoy's fixative (60% methanol, 30% chloroform and 10% acetic acid). Tissues were embedded in paraffin and sectioned into 4 μm slices. Then sections were dewaxed, hydrated and incubated in hybridization buffer (750mM NaCl, 100mM Tris-HCl (pH 7.4), 5 mM EDTA, 0.01% BSA, 10% dextran sulfate) added with pan-bacterial Cy3 conjugated FISH probe EUB338 (5'-GCTGCCTCCCGTAGGAGT-3') at 40°C for 16 h. Sections were washed in wash buffer (50mM NaCl, 4mM Tris-HCl (pH 7.4), 0.02mM EDTA) at 45°C for 10 min for 3 times, followed with counterstained with DAPI and FITC conjugated WGA.

Liquid chromatography–mass spectrometry

Metabolites were analyzed by LC-MS/MS using a system consisting of ACQUITY UPLC BEH C18 column (100 mm*2.1 mm, 1.7μm, Waters, USA) and QExactive HF mass spectrometer (Thermo Fisher Scientific). The analysis was operated in positive and negative electrospray ionization (ESI) mode. ESI settings were as follows: Ion Source Gas1: 60, Ion Source Gas2: 60, Curtain gas: 30, source temperature: 320°C, IonSapary Voltage Floating (ISVF) ± 3500 V. The mass spectrometry settings were as follows: MS scan m/z range: 80-1200 Da, production scan resolution: 17500, MS scan accumulation time 0.20 s/spectra, product ion scan accumulation time 0.05 s/spectra. Data from LC-MS/MS was analyzed with Compound Discoverer 3.0 (Thermo Fisher Scientific) and searched in Bio cyc, HMDB, metlin, HFMDB, Lipidmaps databases.

Mucus thickness measurement

8∼12 week-old mice were sacrificed and distal colons were collected without washing. Tissues were immediately fixed in methacarn solution (60% methanol, 30% chloroform and 10% acetic acid) at room temperature for 24-48 hours. Tissues were twice washed continuously with methanol, ethanol and xylene for 30 min each. Then tissues were paraffin embedded and cut into 4 μm sections. To measure the mucus thickness, sections were dewaxed and hydrated, and then were stained using a combination of Alcian Blue and Periodic acid-Schiff (AB/PAS) stains or stained with FITC conjugated WGA and DAPI. Bright field or fluorescence imaging of sections were collected with Nikon A1R+ confocal microscope. For AB/PAS staining, mucus was stained as blue color. For fluorescence imaging, mucus was detected by FITC conjugated WGA, and epithelial boundary was identified by DAPI signal. Thickness of mucus layer at 30 different sites of each sample was measured and average thickness was calculated.

Microarray assay and bioinformatic analysis

3×10^{5} $Sh2d6^{+}$ Tuft-2 cells ($EGFP^{+}EpCAM^{+}Siglec\text{-}F^{+}$), $Sh2d6^{-}$ Tuft cells ($EGFP^{-}EpCAM^{+}Siglec\text{-}F^{+}$) and non-Tuft-2 epithelial cells ($EGFP^{-}EpCAM^{+}$) from $Sh2d6^{EGFP}$ mice were sorted using flow cytometer and cells were digested with TRIzol reagent. RNA quality

was monitored using NanoDrop ND-1000. RNA integrity was tested by agarose gel electrophoresis. RNA samples were then assayed with Affymetrix Mouse Transcriptome Array 1.0 (Beijing Cnkingbio Biotechnology). R packages of 'ggplot2', 'clusterProfiler' in Bioconductor were used for generating GO analysis.

For bioinformatic analysis of single cell RNA sequencing of Tuft cells, scRNA-seq data was from GSE92332 (Haber et al., 2017). 'Seurat' was used for clustering and finding out signature genes of each cluster. Highly variable genes were identified by using the 'FindVariableFeatures' function. Dimensionality reduction was performed by principal-component analysis using the 'RunPCA' function and principal components (PCs) 1–8 were chosen for further analysis based on the 'JackStrawPlot' and 'ElbowPlot' functions. Cells were clustered using the 'FindNeighbors' function with a k.param of 30 and the 'FindClusters' function with a resolution of 1.2. Cells were then plotted using the t-SNE method. Differently expressed genes were calculated through the 'FindMarkers' function with parameters min.pct = 0.1 and logfc.threshold = 0.25.

'Monocle3' was used for single-cell trajectory analysis. The data was performed using the 'preprocess_cds' function with default parameters. Dimensionality reduction was performed with the 'reduce_dimension' function using UMAP. Finally, trajectory was constructed using the 'cluster_cells' function (parameters: reduction_method = "UMAP", resolution = 0.3, k = 30) and the 'learn_graph' function with use_partition parameter set to FALSE.

QUANTIFICATION AND STATISTICAL ANALYSIS

Number of mice and experiments, and statistical tests are reported in each figure legend. For statistical analysis, data were analyzed by GraphPad Prism 8. Results are shown as means ±SEM. Two-tailed unpaired Student's t-test was used in this study. For survival and time course data, unpaired test was used. *P*-values < 0.05 were considered significant (*, $P < 0.05$; **, $P < 0.01$; ***, $P < 0.001$); $P > 0.05$, non-significant (NS).